Chance-Constrained OPF in Microgrids: A Data-Driven Distributionally Robust Approach with Droop Control and Power Flow Routers

Abhinav Karn, Kris Keshav, Lakhote Pranad Nilesh, Shashank Shekhar, Shivam Bansal
Department of Electrical Engineering, Indian Institute of Technology Roorkee

Abstract

The increasing penetration of renewable energy sources introduces significant uncertainty in the operation of microgrids. Microgrids which use droop-controlled inverter-based distributed generators (DGs) are prone to high voltage volatility. Although droop control enables power sharing without communication, high droop gains significantly increase voltage sensitivity to renewable power fluctuations, leading to voltage volatility and infeasibility of deterministic optimal power flow (OPF). Recently, Chance-constrained OPF (CC-OPF) is being used as an effective method to handle the uncertainty in the system by enforcing probabilistic bounds on operational constraints.

Our base paper uses CC-OPF for droop-controlled microgrids and incorporates power flow routers (PFR) to mitigate voltage volatility. PFRs are power-electronic devices installed on distribution lines that regulate voltage magnitudes and phase angles, thus reducing voltage variance. The paper uses CC-OPF models based on the assumption that renewable forecast errors follow Gaussian distribution. However, renewable generation data usually exhibits non-Gaussian features, and relying on purely Guassian distributions can lead to non-optimal decisions.

In our work, we will extend the existing CC-OPF framework by using Distributionally Robust Optimization (DRO) and data-driven methods. We construct ambiguity sets using empirical renewable generation data and optimize system performance against the worst-case distribution within these sets. This approach makes the system reliable and robust while also avoiding excessive conservatism. The optimization problem is partially linearized to make it computationally feasible. An iterative solution algorithm is used to solve the resulting formulation, and the resulting constraints are reformulated into semidefinite programming (SDP) problem.

We will be showing numerical studies to compare the proposed DRO based approach to Gaussian-based CC-OPF. The use of DRO and PFRs is expected to significantly reduce voltage volatility, enabling more secure and economical operation of droop-controlled microgrids with high renewable penetration.

Chance-Constrained OPF in Droop-Controlled Microgrids With Power Flow Routers

Tianlun Chen, *Member, IEEE*, Yue Song, *Member, IEEE*, David J. Hill, *Life Fellow, IEEE*, and Albert Y. S. Lam, *Senior Member, IEEE*

***Abstract*—High penetration of renewable generation poses challenges to power system operation due to its uncertain nature. In droop-controlled microgrids, the voltage volatility induced by renewable uncertainties is aggravated by the high droop gains. This paper proposes a chance-constrained optimal power flow (CC-OPF) problem with power flow routers (PFRs) to better regulate the voltage profile in microgrids. PFR refers to a general type of network-side controller that brings more flexibility to the power network. Comparing with the normal CC-OPF that relies on node power flexibility only, the proposed model introduces a new dimension of control from power network to enhance system performance under renewable uncertainties. Adopting a partial linearization method and an iterative algorithm allows us to address the CC-OPF problem by iteratively solving a subproblem. Since the inclusion of PFRs complicates the subproblem and makes common solvers no longer applicable directly, a semidefinite programming relaxation is used to transform each subproblem into a convex form. The proposed method is verified on a modified IEEE 33-bus system and the results show that PFRs significantly reduce the standard deviations of voltage magnitudes and contribute to mitigating the voltage volatility, which makes the system operate in a more economic and secure way.**

***Index Terms*—Power flow router, droop-controlled microgrid, chance constraints, optimal power flow, voltage regulation.**

I. Introduction

MICROGRIDS (MGs) refer to low-voltage or medium-voltage power networks integrated with renewable distributed generations (DGs), loads and other control devices [1], which can operate in either grid-connected mode or islanded mode. MGs have drawn much attention in the recent decades due to their flexibility for arbitrary configurations with different sizes and functionalities. However, the high penetration of renewable DGs has brought many challenges to MG operators in handling the economic and security issues. Commonly, islanded MGs adopt droop control schemes for autonomous power sharing between the dispatchable DGs [2]. High droop gains are usually used for better transient response and proper power sharing [3], [4]. However, this feature makes the voltages even more sensitive to power injection changes and leads to highly volatile voltages under renewable uncertainties [5].

Optimal power flow (OPF) is a fundamental tool for voltage regulation and economic dispatch in power system operations. Traditionally, OPF is formulated as a deterministic problem, which optimizes an objection function (e.g., generation cost) subjected to operational constraints such as voltage and line flow limits [6]. However, the deterministic OPF is not sufficient to ensure an economic and secure operation with the presence of uncertainties, especially for droop-controlled MGs where the voltage volatility (i.e., the degree of voltage variance under uncertainties) is further aggravated by the high droop gains. Recently, chance-constrained OPF (CC-OPF) has become a powerful tool for addressing the challenges brought by high penetration of renewables [7], [8]. Different from the deterministic OPF, CC-OPF replaces the hard constraints by chance constraints to guarantee that the probabilities of constraint violations under uncertain disturbances are kept within pre-defined values. Existing studies have shown the effectiveness of CC-OPF in accommodating renewable energy in low voltage systems. For example, the reactive power support from DG inverters is utilized to mitigate voltage variations under renewable uncertainties by chance constrained optimization [9]–[11]. Controllable loads are also utilized through chance constrained framework to achieve a more economic generation and reserve scheduling [12] or reduce the power losses while maintaining an acceptable voltage profile [13]. In another line of work, multi-period optimization [14] and model predictive control [15] are designed with chance constraints using battery energy storage systems (BESSs) to hedge the negative impacts of renewable uncertainties.

The above CC-OPF models mainly rely on node power flexibility provided by node power devices. However, security issues induced by the renewable uncertainties push the system operation much closer to its technical limits and further restrict the effectiveness of node power flexibility. Therefore,

Manuscript received May 18, 2021; revised October 21, 2021 and February 4, 2022; accepted February 19, 2022. Date of publication February 25, 2022; date of current version June 21, 2022. This work was supported in part by the Hong Kong RGC General Research Fund under Project 17209219 and Project 17207918, and in part by the HKU Seed Fund for Basic Research for New Staff under Project 202009185007. Paper no. TSG-00777-2021. *(Corresponding author: Yue Song.)*

Tianlun Chen and Yue Song are with the Department of Electrical and Electronic Engineering, The University of Hong Kong, Hong Kong (e-mail: tlchen@eee.hku.hk; yuesong@eee.hku.hk).

David J. Hill is with the Department of Electrical and Electronic Engineering, The University of Hong Kong, Hong Kong, and also with the School of Electrical Engineering and Telecommunications, The University of New South Wales, Kensington, NSW 2052, Australia (e-mail: dhill@eee.hku.hk).

Albert Y. S. Lam is with the Department of Electrical and Electronic Engineering, The University of Hong Kong, Hong Kong, and also with Fano Labs, Hong Kong (e-mail: ayslam@eee.hku.hk).

Color versions of one or more figures in this article are available at https://doi.org/10.1109/TSG.2022.3154151.

Digital Object Identifier 10.1109/TSG.2022.3154151

network flexibility, which has been proposed in some pioneering works [16], is becoming increasingly important as a considerable supplement to node power flexibility. It introduces a new mechanism into system control that tunes the network parameters to change the routings of power flows, which is different from the conventional node power flexibility that modifies the power injections directly. Thanks to the development of power electronic devices, nowadays power systems have increasing network flexibility. For instance, in high-voltage (HV) transmission systems, HVDC tie-line power control [17]–[19] and phase shifting transformers [17], [20] have been considered in CC-OPF formulations to provide corrective control for lower operational cost without sacrificing the system security. In low-voltage (LV) systems, a representative example of a network controller is the power flow router (PFR), which was first proposed in [21] as a general type of series controller installed at lines that makes power network more flexible. In our previous work [22], tuning PFRs was introduced as an effective way to reduce the BESS capacity required for accommodating renewable energy. The results in [22] indicate that network flexibility may have great potential in voltage regulation in the corresponding multi-period OPF problem. Inspired by these results, we introduce PFRs in MGs to further investigate their capability on addressing voltage volatility issues caused by renewable uncertainties.

In view of the aforementioned issues, we propose a CC-OPF problem in droop-controlled MGs with PFRs to hedge against the renewable uncertainties. Different from the traditional methods that reply on node power flexibility only, the proposed model introduces PFRs that bring extra flexibility into the power network and the role of network flexibility in voltage regulation is firstly revealed. The contributions of this paper are twofold.

1) To the authors' knowledge, this is the first formulation of AC CC-OPF considering MG droop characteristics and network flexibility. We combine the CC-OPF model with the droop characteristics and PFRs; PFRs introduce a new dimension of control which is shown to make significant contribution to the voltage volatility reduction. It leads to a more economic and secure operating status against renewable uncertainties.
2) We extend the solution method in [23] to be compatible with CC-OPF problems with flexible network parameters. Following the spirit of an analytical reformulation of a partially linearized model and an iterative algorithm in [23] allows us to address the CC-OPF problem by iteratively solving a subproblem that retains the basic structure of deterministic AC-OPF. However, PFRs complicate the subproblem by introducing flexible network parameters, which makes it intractable under common AC-OPF solvers. To handle this issue, a semidefinite programming (SDP) relaxation method from [21] is adopted to transform the subproblem into a convex form so that the computationally tractability is achieved.

The remainder of this paper is organized as follows. Section II provides the system modelling and the optimization problem formulation. Section III describes the solution methodology. In Section IV, case studies are presented to evaluate the performance of the proposed model and algorithm. Finally, conclusions and future work are given in Section V.

II. Problem Formulation

Consider an islanded MG with n buses and l lines. Let $\mathcal{N} \coloneqq \{1, 2, \ldots, n\}$ the set of buses and $\mathcal{E} \subseteq \mathcal{N} \times \mathcal{N}$ be the set of lines. Each bus may connect a dispatchable DG, a renewable DG and a load. For bus i, the active and reactive power generation outputs of the dispatchable DG are denoted as P_{G_i} and Q_{G_i}; the active and reactive power generation outputs of the renewable DG are denoted as P_{W_i} and Q_{W_i}; the active and reactive power loads are denoted as P_{L_i} and Q_{L_i}. For bus k without DG generations or loads, the respective notations P_{G_k}, Q_{G_k}, P_{W_k}, Q_{W_k}, P_{L_k}, Q_{L_k} are always zero. Also, denote V_i and θ_i as the voltage magnitude and voltage angle at bus i. Without loss of generality, we take bus 1 as the angle reference bus and make θ_1 fixed to zero. A line connecting bus i and bus j is denoted by an unordered pair $(i, j) \in \mathcal{E}$. A line with PFRs is denoted as $(i, j) \in \mathcal{E}^{\text{pfr}} \subseteq \mathcal{E}$ and let $\mathcal{E}^{\text{norm}} = \mathcal{E} \setminus \mathcal{E}^{\text{pfr}}$ be the set of normal lines without PFRs. Let the set of neighboring buses of bus $i \in \mathcal{N}$ as $\mathcal{N}_i = \{j \in \mathcal{N} \mid (i, j) \in \mathcal{E}\}$, which also means that bus i and bus j are connected by the line (i, j). For matrix $\boldsymbol{A}$, we denote its Hermitian (conjugate) transpose by $\boldsymbol{A}^H$. In the following, we detail the system models and the optimization problem formulation.

A. Droop-Controlled Dispatchable DGs

A dispatchable DG refers to a DG unit whose output can be adjusted by the operators. We denote the set of buses with dispatchable DG generations as $\mathcal{N}_{\mathcal{G}} \in \mathcal{N}$. The dispatchable DGs are assumed to adopt the conventional P-ω and Q-V droop control [5], which is expressed as

$$P_{G_i} = P^*_{G_i} + K^{-1}_{p_i}\left(\omega^* - \omega\right), i \in \mathcal{N}_{\mathcal{G}} \tag{1a}$$

$$Q_{G_i} = Q^*_{G_i} + K^{-1}_{q_i}\left(V^*_i - V_i\right), i \in \mathcal{N}_{\mathcal{G}} \tag{1b}$$

where ω is the angular frequency of the system; ω^* and V^*_i are the set points of frequency and voltage magnitude; K_{p_i} and K_{q_i} are the frequency and voltage droop gains; $P^*_{G_i}$ and $Q^*_{G_i}$ are the set points of active and reactive power generation.

Moreover, the actual active and reactive outputs of dispatchable DGs should be within their capability limits, i.e., $\sqrt{P^2_{G_i} + Q^2_{G_i}} \le S^{\max}_{G_i}$. A typical capability curve of dispatchable DG can be described as shown in [24, Fig. 2], which can be linearized as follows

$$\begin{aligned} &0 \le P_{G_i} \le S^{\max}_{G_i}, \\ &-S^{\max}_{G_i} \le \cos\left(m\frac{\pi}{k}\right)P_{G_i} + \sin\left(m\frac{\pi}{k}\right)Q_{G_i} \le S^{\max}_{G_i}, \\ &m = 1, \ldots, k \end{aligned} \tag{2}$$

where the error caused by this linearization can be controlled by adjusting k. As tested in [24], for $k = 16$, the error is negligible and the resulting accuracy is sufficiently high.

B. Renewable DGs and Uncertainty Modeling

A renewable DG is considered as a non-dispatchable source. We assume the renewable DGs follow the maximum power

point tracking mode which introduce uncertainties into the power network. The active power generation of renewable DG at bus i is modelled as sum of the forecasted value $P^f_{W_i}$ and forecast error ξ_i

$$P_{W_i}(\boldsymbol{\xi}) = P^f_{W_i} + \xi_i, \tag{3}$$

where $\boldsymbol{\xi} = [\xi_i] \in \mathbb{R}^n$ is a vector of forecast errors which is assumed to follow a multivariate Gaussian distribution featured by zero mean and known covariance matrix $\Sigma \in \mathbb{R}^{n\times n}$, which can be estimated based on historical data or forecasting techniques [25]. For bus k without renewable DG generation, the corresponding k-th row and column of Σ are set to zero. Moreover, we assume a constant power factor λ_i so that the reactive power generation at bus i follows the active power generation:

$$Q_{W_i}(\boldsymbol{\xi}) = \lambda_i\Big(P^f_{W_i} + \xi_i\Big), \tag{4}$$

where $\lambda_i = \tan\phi_i$ determines the reactive power control of renewable DG at bus i. Similar to above, for bus k without renewable DG generation, λ_k is always zero. For simplicity, we consider the renewable DGs as the only source of power injection uncertainties and our model can be easily extended to include load uncertainties.

Note that Gaussian distribution is one of the most common models to describe the uncertainties of renewable outputs [17], [23], [26]. But the event at the very tails of a Gaussian distribution (e.g., outside the 3 standard deviations) is not realistic since the renewable DG output is physically bounded. Nevertheless, the tailed part of a Gaussian distribution counts nearly zero probability (e.g., the area outside 3 standard deviations covers just 0.27% probability). Thus, it makes almost no difference if the Gaussian distribution is truncated at the very tailed part or not. The possible extension to truncated Gaussian distributions will also be discussed in Section III-F.

C. Power Flow Equations With Power Flow Routers

The AC power flow equations are adopted for accurately describing the behaviours under renewable uncertainties. For a normal line (i, j) without PFRs, the active and reactive branch power flows P_{ij} and Q_{ij} are given as

$$P_{ij} = g_{ij}\Big(V_i^2 - V_iV_j\cos\theta_{ij}\Big) - b_{ij}V_iV_j\sin\theta_{ij}, \tag{5a}$$

$$Q_{ij} = -b_{ij}\Big(V_i^2 - V_iV_j\cos\theta_{ij}\Big) - g_{ij}V_iV_j\sin\theta_{ij}, \tag{5b}$$

where $y_{ij} = g_{ij} + \mathrm{j}b_{ij}$ represents the admittance of line (i, j); the notation θ_{ij} is the short for $\theta_i - \theta_j$.

PFRs are installed at some lines to bring network flexibility to the system and enlarge the feasible region of OPF problems [21], [27]. The diagram of a line with PFRs is shown in Fig. 1. The concept of PFR can be realized by multiple ways. One possible realistic implementation is a pair of power electronic transformers [28] at two terminals of a line, which can actively tune the voltage magnitudes (V_{i_j}, V_{j_i}) and angles $(\theta_{i_j}, \theta_{j_i})$ of their secondary sides. This implementation makes PFRs applicable in both HV and LV systems and it will be natural to introduce PFRs into MGs as power electronics devices are more and more ubiquitous. The authors' previous

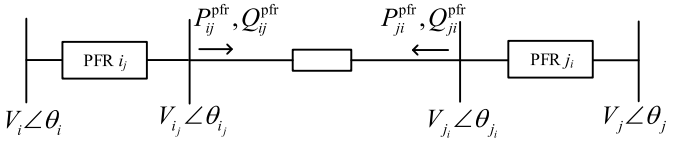

Fig. 1. Diagram of a line with PFRs.

work with colleagues [21], [22], [27] have investigated the value of PFRs in different OPF formulations for loadability enhancement, cost reduction and voltage regulation. Further, it will be seen later that PFRs can benefit CC-OPF for voltage regulation by tuning both the mean values and standard deviations of voltages, while DG generation dispatch is only effective in tuning the mean values.

The branch power flow with PFRs is presented as follows. As shown in Fig. 1, $V_{i_j}\angle\theta_{i_j}$ and $V_{j_i}\angle\theta_{j_i}$ refer to the complex voltages of the secondary sides of the PFRs. The relations between $V_{i_j}\angle\theta_{i_j}$, $V_{j_i}\angle\theta_{j_i}$ and $V_i\angle\theta_i$, $V_j\angle\theta_j$ are given by

$$V_{i_j}\angle\theta_{i_j} = T^*_{i_j}V_i\angle\Big(\theta_i + \beta^*_{i_j}\Big) \tag{6a}$$

$$V_{j_i}\angle\theta_{j_i} = T^*_{j_i}V_j\angle\Big(\theta_j + \beta^*_{j_i}\Big) \tag{6b}$$

where $T^*_{i_j}$ and $T^*_{j_i}$ are the tap ratio set points of PFR i_j and j_i; $\beta^*_{i_j}$ and $\beta^*_{j_i}$ are the phase shift set points of PFR i_j and j_i. The PFRs are assumed to have no conversion losses [21]. Thus, for a line (i, j) with PFRs, the active and reactive branch power flows are expressed as

$$\begin{aligned} P^{\mathrm{pfr}}_{ij} &= g_{ij}\Big(V^2_{i_j} - V_{i_j}V_{j_i}\cos\big(\theta_{i_j} - \theta_{j_i}\big)\Big) \\ &\quad - b_{ij}V_{i_j}V_{j_i}\sin\big(\theta_{i_j} - \theta_{j_i}\big) \\ &= g_{ij}\Big(T^{*2}_{i_j}V_i^2 - T^*_{i_j}T^*_{j_i}V_iV_j\cos\Big(\theta_{ij} + \beta^*_{i_jj_i}\Big)\Big) \\ &\quad - b_{ij}T^*_{i_j}T^*_{j_i}V_iV_j\sin\Big(\theta_{ij} + \beta^*_{i_jj_i}\Big) \end{aligned} \tag{7a}$$

$$\begin{aligned} Q^{\mathrm{pfr}}_{ij} &= -b_{ij}\Big(V^2_{i_j} - V_{i_j}V_{j_i}\cos\big(\theta_{i_j} - \theta_{j_i}\big)\Big) \\ &\quad - g_{ij}V_{i_j}V_{j_i}\sin\big(\theta_{i_j} - \theta_{j_i}\big) \\ &= -b_{ij}\Big(T^{*2}_{i_j}V_i^2 - T^*_{i_j}T^*_{j_i}V_iV_j\cos\Big(\theta_{ij} + \beta^*_{i_jj_i}\Big)\Big) \\ &\quad - g_{ij}T^*_{i_j}T^*_{j_i}V_iV_j\sin\Big(\theta_{ij} + \beta^*_{i_jj_i}\Big) \end{aligned} \tag{7b}$$

where the notation $\beta^*_{i_jj_i}$ is the short for $\beta^*_{i_j} - \beta^*_{j_i}$. For simplicity, branch power flows without PFRs (5a)-(5b) can be transformed into (7a)-(7b) by setting $T^*_{i_j} = T^*_{j_i} = 1$ and $\beta^*_{i_j} = \beta^*_{j_i} = 0$. Thus, the active and reactive power balance at each bus i can be given by the unified expression below

$$P_{G_i} + P_{W_i}(\boldsymbol{\xi}) - P_{L_i} = \sum_{j\in\mathcal{N}_i} P^{\mathrm{pfr}}_{ij}\big(\boldsymbol{V}, \boldsymbol{\theta}, \boldsymbol{T}^*, \boldsymbol{\beta}^*\big) \tag{8a}$$

$$Q_{G_i} + Q_{W_i}(\boldsymbol{\xi}) - Q_{L_i} = \sum_{j\in\mathcal{N}_i} Q^{\mathrm{pfr}}_{ij}\big(\boldsymbol{V}, \boldsymbol{\theta}, \boldsymbol{T}^*, \boldsymbol{\beta}^*\big) \tag{8b}$$

where P_{L_i} and Q_{L_i} are the active and reactive power loads at bus i; $\boldsymbol{V} \in \mathbb{R}^n$ and $\boldsymbol{\theta} \in \mathbb{R}^n$ stack V_i and θ_i, respectively; $\boldsymbol{T}^* := (T^*_{i_j}, T^*_{j_i}, (i, j) \in \mathcal{E})$, $\boldsymbol{\beta}^* := (\beta^*_{i_j}, \beta^*_{j_i}, (i, j) \in \mathcal{E})$. We also

define the vectors $\boldsymbol{P}_G, \boldsymbol{Q}_G, \boldsymbol{P}_W(\boldsymbol{\xi}), \boldsymbol{Q}_W(\boldsymbol{\xi}) \in \mathbb{R}^n$ stacking P_{G_i}, Q_{G_i}, $P_{W_i}(\boldsymbol{\xi})$, $Q_{W_i}(\boldsymbol{\xi})$, respectively.

D. Optimization Problem Formulation

As stated in the previous section, given the set points $\{\boldsymbol{P}_G^*, \boldsymbol{Q}_G^*, \omega^*, \boldsymbol{V}^*, \boldsymbol{T}^*, \boldsymbol{\beta}^*\}$ and renewable power generation $\boldsymbol{P}_W$, $\boldsymbol{Q}_W$, we can determine the values of $\{\boldsymbol{P}_G, \boldsymbol{Q}_G, \boldsymbol{V}, \boldsymbol{\theta}, \omega\}$ based on (1a)-(1b) and (7a)-(8b). Since $\boldsymbol{P}_W$ and $\boldsymbol{Q}_W$ are functions of uncertainty $\boldsymbol{\xi}$, $\{\boldsymbol{P}_G, \boldsymbol{Q}_G, \boldsymbol{V}, \boldsymbol{\theta}, \omega\}$ are not only subject to one possible realization of $\boldsymbol{\xi}$ but to a variety of renewable power realizations. Thus, they can also be expressed as the implicit functions of $\boldsymbol{\xi}$, say $\{\boldsymbol{P}_G(\boldsymbol{\xi}), \boldsymbol{Q}_G(\boldsymbol{\xi}), \boldsymbol{V}(\boldsymbol{\xi}), \boldsymbol{\theta}(\boldsymbol{\xi}), \omega(\boldsymbol{\xi})\}$, which describe the system responses to the uncertainty realizations. Hence, we can formulate the CC-OPF with PFRs (CC-OPF-PFR) as follows

$$\min \ \mathbb{E}\left[\sum_{i\in\mathcal{N}_\mathcal{G}} c_{2i}P_{G_i}(\boldsymbol{\xi})^2 + c_{1i}P_{G_i}(\boldsymbol{\xi}) + c_{0i}\right], \tag{9a}$$

$$s.t. \ \ (7a)-(7b), \tag{9b}$$

$$P_{G_i}(\boldsymbol{\xi}) + P_{W_i}(\boldsymbol{\xi}) - P_{L_i} = \sum_{j\in\mathcal{N}_i} P_{ij}^{\text{pfr}}\big(\boldsymbol{V}(\boldsymbol{\xi}), \boldsymbol{\theta}(\boldsymbol{\xi}), \boldsymbol{T}^*, \boldsymbol{\beta}^*\big), \forall i \in \mathcal{N} \tag{9c}$$

$$Q_{G_i}(\boldsymbol{\xi}) + Q_{W_i}(\boldsymbol{\xi}) - Q_{L_i} = \sum_{j\in\mathcal{N}_i} Q_{ij}^{\text{pfr}}\big(\boldsymbol{V}(\boldsymbol{\xi}), \boldsymbol{\theta}(\boldsymbol{\xi}), \boldsymbol{T}^*, \boldsymbol{\beta}^*\big), \forall i \in \mathcal{N} \tag{9d}$$

$$P_{G_i}(\boldsymbol{\xi}) = P_{G_i}^* + K_{p_i}^{-1}\big(\omega^* - \omega(\boldsymbol{\xi})\big), i \in \mathcal{N}_\mathcal{G} \tag{9e}$$

$$Q_{G_i}(\boldsymbol{\xi}) = Q_{G_i}^* + K_{q_i}^{-1}(V_i^* - V_i(\boldsymbol{\xi})), i \in \mathcal{N}_\mathcal{G} \tag{9f}$$

$$\mathbb{P}\big(P_{G_i}(\boldsymbol{\xi}) \le S_{G_i}^{\max}\big) \ge 1 - \epsilon_G, \forall i \in \mathcal{N}_G \tag{9g}$$

$$\mathbb{P}\big(P_{G_i}(\boldsymbol{\xi}) \ge 0\big) \ge 1 - \epsilon_G, \forall i \in \mathcal{N}_G \tag{9h}$$

$$\mathbb{P}\Big[\cos\Big(m\frac{\pi}{16}\Big)P_{G_i}(\boldsymbol{\xi}) + \sin\Big(m\frac{\pi}{16}\Big)Q_{G_i}(\boldsymbol{\xi}) \ge -S_{G_i}^{\max}\Big] \ge 1 - \epsilon_G, \quad m = 1, \ldots, 16, \ \forall i \in \mathcal{N}_G \tag{9i}$$

$$\mathbb{P}\Big[\cos\Big(m\frac{\pi}{16}\Big)P_{G_i}(\boldsymbol{\xi}) + \sin\Big(m\frac{\pi}{16}\Big)Q_{G_i}(\boldsymbol{\xi}) \le S_{G_i}^{\max}\Big] \ge 1 - \epsilon_G, \quad m = 1, \ldots, 16, \ \forall i \in \mathcal{N}_G \tag{9j}$$

$$\mathbb{P}\big(V_i(\boldsymbol{\xi}) \le V_i^{\max}\big) \ge 1 - \epsilon_V, \forall i \in \mathcal{N} \tag{9k}$$

$$\mathbb{P}\Big(V_i(\boldsymbol{\xi}) \ge V_i^{\min}\Big) \ge 1 - \epsilon_V, \forall i \in \mathcal{N} \tag{9l}$$

$$\mathbb{P}\big(\omega(\boldsymbol{\xi}) \le \omega^{\max}\big) \ge 1 - \epsilon_\omega, \tag{9m}$$

$$\mathbb{P}\Big(\omega(\boldsymbol{\xi}) \ge \omega^{\min}\Big) \ge 1 - \epsilon_\omega, \tag{9n}$$

$$P_{G_i}^{\min} \le P_{G_i}^* \le P_{G_i}^{\max}, \forall i \in \mathcal{N}_\mathcal{G} \tag{9o}$$

$$Q_{G_i}^{\min} \le Q_{G_i}^* \le Q_{G_i}^{\max}, \forall i \in \mathcal{N}_\mathcal{G} \tag{9p}$$

$$V_i^{\min} \le V_i^* \le V_i^{\max}, \forall i \in \mathcal{N} \tag{9q}$$

$$\omega^{\min} \le \omega^* \le \omega^{\max}, \tag{9r}$$

$$T_{ij}^{\min} \le T_{ij}^* \le T_{ij}^{\max}, T_{ji}^{\min} \le T_{ji}^* \le T_{ji}^{\max}, \forall (i,j) \in \mathcal{E}^{\text{pfr}} \tag{9s}$$

$$\beta_{ij}^{\min} \le \beta_{ij}^* \le \beta_{ij}^{\max}, \beta_{ji}^{\min} \le \beta_{ji}^* \le \beta_{ji}^{\max}, \forall (i,j) \in \mathcal{E}^{\text{pfr}} \tag{9t}$$

$$T_{ij}^* = T_{ji}^* = 1, \quad \beta_{ij}^* = \beta_{ji}^* = 0^{\text{o}}, \quad \forall (i,j) \in \mathcal{E}^{\text{norm}} \tag{9u}$$

$$\theta_1 = 0^{\text{o}}. \tag{9v}$$

In this formulation, the objective function (9a) is to minimize the expected generation cost of the dispatchable DGs, where c_{2i}, c_{1i}, c_{0i} are the cost coefficients. Constraints (9b)–(9f) describe the power balance equations with PFRs and droop characteristics. Constraints (9g)–(9j) are the chance constraints for active power and reactive power generation of dispatchable DGs. Constraints (9k)–(9n) are the chance constraints for voltage magnitudes and system frequency. Chance constraint restricts the feasible region of OPF to a desired confidence region. In other words, it ensures the probability of constraint violation under any realization of uncertainties to be lower than a pre-specified level ϵ. Constraints (9o)–(9r) give the limits for set points of power outputs of dispatchable DGs, voltage magnitudes and system frequency, respectively. Constraints (9s)–(9u) represent the upper and lower limits for tuning variables of PFRs and specific settings for normal lines. We denote bus 1 as the reference bus and make θ_1 fixed to zero in (9v).

One major advantage of the CC-OPF-PFR model is that the generation dispatch is coordinated with PFR tuning to regulate voltages under renewable uncertainties. According to [3], the values of droop gains are usually large in MGs. However, this setting may result in volatile voltages and even make CC-OPF infeasible. On the other hand, it will be seen that the employment of PFRs considerably reduces voltage volatility.

Note that the set points $\{\boldsymbol{P}_G^*, \boldsymbol{Q}_G^*, \omega^*, \boldsymbol{V}^*, \boldsymbol{T}^*, \boldsymbol{\beta}^*\}$ are determined by problem (9) and remain constant under renewable generation fluctuations. Hence, the chance constraints (9k)–(9n) refer to the system responses with the fixed set points under different renewable output scenarios and need to be satisfied with the prescribed violation probabilities.

Remark 1: The time scale considered in this paper is steady-state, e.g., the system snapshot in each 15-min window, and hence the frequency in problem (9) refers to the steady-state frequency. In islanded MGs, all dispatchable DGs do not have large capacities so that there is no slack bus capable of maintaining the nominal frequency [29]–[31]. Moreover, in case that all DGs are droop-controlled inverter-based and no other frequency recovery techniques are applied, then it will be true that the steady-state frequency may not be exactly equal to the nominal value. This viewpoint has been adopted in many existing literature [32]–[34], where the frequency is treated as a variable in MG OPF and the frequency is enforced to be within a narrow interval to bound the deviation. This setting makes sense as a fully inverter-based MG is not required to operate at exactly the nominal frequency, which is different from the systems with synchronous generators.

Remark 2: In the conventional transmission systems, spinning reserves of synchronous generators are engaged to balance the supply and demand timely [17], [35], [36]. However, the situation is different in droop-controlled MGs as the DG inverters can ramp up/down to follow the fluctuations in a more flexible way than synchronous generators. Thus, the DG capacity limits are sufficient to capture the dispatchability of DG inverters, and the reserve term is not needed in the proposed model.

III. Solution Methodology

There exist two difficulties in solving problem (9). The first one is that the non-linearity of power flow equations introduces significant challenges to quantify the system behaviours under renewable uncertainties. To address this issue, we follow

the spirit of a partial linearization approach with an iterative solution algorithm proposed in [23]. Here the partial linearization means we apply linearization only in part of the manipulations. We adopt the AC power flow equations for the forecasted renewable output scenario and then linearize the AC power flow equations by using a first-order Taylor expansion around a given operating point to model the system responses under forecast errors. This linearization is justified by the fact that the renewable forecast techniques have been developed with satisfactory performance so that the forecast errors are quite small. Therefore, we can expect this approach to provide sufficiently accurate results, e.g., on the evaluation of the probability density functions (PDFs) of system states including voltage magnitudes and generation outputs. The partial linearization approach enables the analytical reformulation of chance constraints and also leads to a more tractable form of problem (9). Then, the iterative solution algorithm [23] is adopted to address the reformulated problem by iteratively solving a subproblem which retains the basic structure of deterministic AC-OPF.

The second difficulty arises due to the consideration of PFRs. The solution method in [23] is designed for CC-OPF problems with fixed network parameters, which does not directly apply to our model where some network parameters also become variables with the presence of PFRs. The flexible network parameters complicate the subproblem in the above-mentioned iterative algorithm, which makes common OPF solvers no longer apply. To address this issue,a modified SDP relaxation method [21] is adopted to solve the subproblem, which extends the iterative solution framework to be compatible with CC-OPF problems containing flexible network parameters. In the following, we will detail the solution method.

A. Power Flow Linearization

As stated in Section II, we can obtain an operating point $(\boldsymbol{V}, \boldsymbol{\theta}, \omega)$ under the forecasted renewable output scenario $\boldsymbol{\xi} = \boldsymbol{0}$ and certain set points $\{\boldsymbol{P}_G^*, \boldsymbol{Q}_G^*, \omega^*, \boldsymbol{V}^*, \boldsymbol{T}^*, \boldsymbol{\beta}^*\}$. This operating point satisfies the power flow equations (9b)-(9f) which are rewritten into a compact form for simplicity

$$\boldsymbol{f}\big(\boldsymbol{P}_W(\boldsymbol{0}), \boldsymbol{Q}_W(\boldsymbol{0}), \boldsymbol{V}(\boldsymbol{0}), \boldsymbol{\theta}(\boldsymbol{0}), \omega(\boldsymbol{0})\big) = \boldsymbol{0}. \tag{10}$$

Linearizing (10) around the given operating point gives the relation between the change of renewable power generations (i.e., $\boldsymbol{\xi}$ with small values) and the change of voltages and frequency

$$\begin{bmatrix} \Delta \boldsymbol{P}_W \\ \Delta \boldsymbol{Q}_W \\ 0 \end{bmatrix} = \boldsymbol{J}_{PF} \begin{bmatrix} \Delta \boldsymbol{\theta} \\ \Delta \boldsymbol{V} \\ \Delta \omega \end{bmatrix}, \tag{11}$$

where the notation Δ denotes the deviation from the given operating point and we define $\Delta \boldsymbol{P}_W = [\Delta P_{W_i}]$, $\Delta \boldsymbol{Q}_W = [\Delta Q_{W_i}]$, $\Delta \boldsymbol{V} = [\Delta V_i]$, $\Delta \boldsymbol{\theta} = [\Delta \theta_i] \in \mathbb{R}^n$. Also, we denote $\boldsymbol{J}_{PF} \in \mathbb{R}^{(2n+1)\times(2n+1)}$ as the Jacobian matrix which can be expressed as

$$\boldsymbol{J}_{PF} = \begin{bmatrix} \boldsymbol{A} & \boldsymbol{B} & \boldsymbol{S}_P \\ \boldsymbol{C} & \boldsymbol{D} + \boldsymbol{S}_Q & \boldsymbol{0} \\ \boldsymbol{e}_1 & \boldsymbol{0} & \boldsymbol{0} \end{bmatrix}. \tag{12}$$

where the last row of $\boldsymbol{J}_{PF}$ represents the reference bus angle is being fixed to zero; $\boldsymbol{S}_P = [S_{P_i}] \in \mathbb{R}^n$ is defined such that $S_{P_i} = K_{P_i}^{-1}, i \in \mathcal{N}_\mathcal{G}$ and $S_{P_i} = 0, i \in \mathcal{N} \setminus \mathcal{N}_\mathcal{G}$. For simplicity, a diagonal matrix $\boldsymbol{H} = \mathrm{diag}\{h_1, h_2, \ldots, h_p\} \in \mathbb{R}^{p\times p}$ is denoted as $\boldsymbol{H} = \mathrm{diag}\{h_i\} \in \mathbb{R}^{p\times p}$. Then, we define $\boldsymbol{S}_Q$ as $\boldsymbol{S}_Q = \mathrm{diag}\{S_{Q_i}\} \in \mathbb{R}^{n\times n}$ such that $S_{Q_i} = K_{Q_i}^{-1}, i \in \mathcal{N}_\mathcal{G}$ and $S_{Q_i} = 0, i \in \mathcal{N} \setminus \mathcal{N}_\mathcal{G}$. The sub-matrix $\boldsymbol{e}_1$ represents the vector with the first entry being one and the other entries being zero. The sub-matrices $\boldsymbol{A}, \boldsymbol{B}, \boldsymbol{C}, \boldsymbol{D} \in \mathbb{R}^{n\times n}$ are derived from the power flow equations (1a)–(1b) and (8a)–(8b). The detailed expressions of $(\boldsymbol{A})_{ij}$, $(\boldsymbol{B})_{ij}$, $(\boldsymbol{C})_{ij}$, $(\boldsymbol{D})_{ij}$ are as follows

$$(\boldsymbol{A})_{ij} = \begin{cases} \sum_{k=1}^n \Big(g_{ik} T_{i_k}^* T_{k_i}^* V_i V_k \sin\Big(\theta_{ik} + \beta_{i_k k_i}^*\Big) \\ \qquad - b_{ik} T_{i_k}^* T_{k_i}^* V_i V_k \cos\Big(\theta_{ik} + \beta_{i_k k_i}^*\Big)\Big), i = j \\ g_{ij} T_{i_j}^* T_{j_i}^* V_i V_j \sin\Big(\theta_{ij} + \beta_{i_j j_i}^*\Big) \\ \qquad + b_{ij} T_{i_j}^* T_{j_i}^* V_i V_j \cos\Big(\theta_{ij} + \beta_{i_j j_i}^*\Big), i \neq j \end{cases}$$

$$(\boldsymbol{B})_{ij} = \begin{cases} \sum_{k=1}^n \Big(g_{ik} \Big(2T_{i_k}^* V_i - T_{k_i}^* V_k \cos\Big(\theta_{ik} + \beta_{i_k k_i}^*\Big)\Big) \\ \qquad - b_{ik} T_{k_i}^* V_k \sin\Big(\theta_{ik} + \beta_{i_k k_i}^*\Big)\Big), i = j \\ g_{ij} \Big(-T_{i_j}^* V_i \cos\Big(\theta_{ij} + \beta_{i_j j_i}^*\Big)\Big) \\ \qquad - b_{ij} T_{i_j}^* V_i \sin\Big(\theta_{ij} + \beta_{i_j j_i}^*\Big), i \neq j \end{cases} \tag{13}$$

$$(\boldsymbol{C})_{ij} = \begin{cases} \sum_{k=1}^n \Big(-b_{ik} T_{i_k}^* T_{k_i}^* V_i V_k \sin\Big(\theta_{ik} + \beta_{i_k k_i}^*\Big) \\ \qquad - g_{ik} T_{i_k}^* T_{k_i}^* V_i V_k \cos\Big(\theta_{ik} + \beta_{i_k k_i}^*\Big)\Big), i = j \\ -b_{ij} T_{i_j}^* T_{j_i}^* V_i V_j \sin\Big(\theta_{ij} + \beta_{i_j j_i}^*\Big) \\ \qquad + g_{ij} T_{i_j}^* T_{j_i}^* V_i V_j \cos\Big(\theta_{ij} + \beta_{i_j j_i}^*\Big), i \neq j \end{cases}$$

$$(\boldsymbol{D})_{ij} = \begin{cases} \sum_{k=1}^n \Big(-b_{ik} \Big(2T_{i_k}^* V_i - T_{k_i}^* V_k \cos\Big(\theta_{ik} + \beta_{i_k k_i}^*\Big)\Big) \\ \qquad - g_{ik} T_{k_i}^* V_k \sin\Big(\theta_{ik} + \beta_{i_k k_i}^*\Big)\Big), i = j \\ -b_{ij} \Big(-T_{i_j}^* V_i \cos\Big(\theta_{ij} + \beta_{i_j j_i}^*\Big)\Big) \\ \qquad - g_{ij} T_{i_j}^* V_i \sin\Big(\theta_{ij} + \beta_{i_j j_i}^*\Big), i \neq j. \end{cases}$$

From the above equations we derive the expressions for the changes of system frequency and voltages with respect to renewable power fluctuations:

$$\begin{bmatrix} \Delta \boldsymbol{\theta} \\ \Delta \boldsymbol{V} \\ \Delta \omega \end{bmatrix} = \boldsymbol{J}_{inv} \begin{bmatrix} \Delta \boldsymbol{P}_W \\ \Delta \boldsymbol{Q}_W \\ 0 \end{bmatrix}. \tag{14}$$

Substituting (4) to (14) and dividing $\boldsymbol{J}_{inv}$ to sub-matrices give

$$\begin{bmatrix} \Delta \boldsymbol{\theta} \\ \Delta \boldsymbol{V} \\ \Delta \omega \end{bmatrix} = \begin{bmatrix} \boldsymbol{J}_{inv}^{11} & \boldsymbol{J}_{inv}^{12} & \boldsymbol{J}_{inv}^{13} \\ \boldsymbol{J}_{inv}^{21} & \boldsymbol{J}_{inv}^{22} & \boldsymbol{J}_{inv}^{23} \\ \boldsymbol{J}_{inv}^{31} & \boldsymbol{J}_{inv}^{32} & \boldsymbol{J}_{inv}^{33} \end{bmatrix} \begin{bmatrix} \Delta \boldsymbol{P}_W \\ \boldsymbol{\lambda} \Delta \boldsymbol{P}_W \\ 0 \end{bmatrix}, \tag{15}$$

where $\boldsymbol{\lambda} = \mathrm{diag}(\lambda_i) \in \mathbb{R}^{n\times n}$; $\boldsymbol{J}_{inv}$ is the inversion of Jacobian matrix $\boldsymbol{J}_{PF}$ and it can be divided into sub-matrices $\boldsymbol{J}_{inv}^{11}, \boldsymbol{J}_{inv}^{12}, \boldsymbol{J}_{inv}^{21}, \boldsymbol{J}_{inv}^{22} \in \mathbb{R}^{n\times n}$, $\boldsymbol{J}_{inv}^{31}, \boldsymbol{J}_{inv}^{32} \in \mathbb{R}^{1\times n}$, $\boldsymbol{J}_{inv}^{13}, \boldsymbol{J}_{inv}^{23} \in \mathbb{R}^n$ and $\boldsymbol{J}_{inv}^{33} \in \mathbb{R}$. The above equations allow us to obtain the following expressions for $\Delta \boldsymbol{V}$ and $\Delta \omega$

$$\Delta \boldsymbol{V} = \boldsymbol{L}_V \Delta \boldsymbol{P}_W, \quad \Delta \omega = \boldsymbol{L}_\omega \Delta \boldsymbol{P}_W, \tag{16}$$

where $\boldsymbol{L}_V \in \mathbb{R}^{n\times n}$ and $\boldsymbol{L}_\omega \in \mathbb{R}^{1\times n}$ represent the sensitivities of voltage magnitudes and frequency to $\Delta \boldsymbol{P}_W$, respectively; $\boldsymbol{L}_V$

and $\boldsymbol{L}_\omega$ can be calculated by

$$\boldsymbol{L}_V = \boldsymbol{J}_{inv}^{21} + \boldsymbol{\lambda}\boldsymbol{J}_{inv}^{22},\ \boldsymbol{L}_\omega = \boldsymbol{J}_{inv}^{31} + \boldsymbol{\lambda}\boldsymbol{J}_{inv}^{32}. \tag{17}$$

Based on the chain rule and the droop characteristics we have

$$\Delta\boldsymbol{P}_G = \frac{\partial \boldsymbol{P}_G}{\partial \omega}\Delta\omega = -\boldsymbol{S}_P\boldsymbol{L}_\omega\Delta\boldsymbol{P}_W \triangleq \boldsymbol{L}_P\Delta\boldsymbol{P}_W, \tag{18}$$

$$\Delta\boldsymbol{Q}_G = \frac{\partial \boldsymbol{Q}_G}{\partial \boldsymbol{V}}\Delta\boldsymbol{V} = -\boldsymbol{S}_Q\boldsymbol{L}_V\Delta\boldsymbol{P}_W \triangleq \boldsymbol{L}_Q\Delta\boldsymbol{P}_W, \tag{19}$$

where $\boldsymbol{L}_P \in \mathbb{R}^{n\times n}$ and $\boldsymbol{L}_Q \in \mathbb{R}^{n\times n}$ represent the sensitivities of active and reactive power generation of dispatchable DGs.

Based on above equations, the sensitivity matrices $\boldsymbol{L}_P, \boldsymbol{L}_Q, \boldsymbol{L}_V, \boldsymbol{L}_\omega$ can be derived, which characterize the system responses under small uncertainties $\boldsymbol{\xi}$. Note that the sensitivity matrices are implicit and nonlinear functions of decision variables $\{\boldsymbol{V}, \boldsymbol{\theta}, \boldsymbol{T}^*, \boldsymbol{\beta}^*\}$ since they are given by the inversion of $\boldsymbol{J}_{PF}$.

B. Analytical Reformulation of Chance Constraints

Next, we further derive an analytical reformulation of the chance constraints based on the assumption that the PDF of renewable uncertainty $\boldsymbol{\xi}$ is a multivariate Gaussian distribution, with zero mean value and known covariance matrix Σ. First, using the sensitivity matrices $\boldsymbol{L}_P, \boldsymbol{L}_Q, \boldsymbol{L}_V, \boldsymbol{L}_\omega$, chance constraints (9g)–(9n) can be approximated as linear functions of renewable uncertainties

$$\mathbb{P}\big(P_{G_i}(\mathbf{0}) + \boldsymbol{L}_{P(i,\cdot)}\boldsymbol{\xi} \le S_{G_i}^{\max}\big) \ge 1-\epsilon_G, \quad \forall i \in \mathcal{N}_\mathcal{G} \tag{20}$$

$$\mathbb{P}\big(P_{G_i}(\mathbf{0}) + \boldsymbol{L}_{P(i,\cdot)}\boldsymbol{\xi} \ge 0\big) \ge 1-\epsilon_G, \quad \forall i \in \mathcal{N}_\mathcal{G} \tag{21}$$

$$\mathbb{P}\big(a\big(P_{G_i}(\mathbf{0}) + \boldsymbol{L}_{P(i,\cdot)}\boldsymbol{\xi}\big) + b\big(Q_{G_i}(\mathbf{0}) + \boldsymbol{L}_{Q(i,\cdot)}\boldsymbol{\xi}\big) \le S_{G_i}^{\max}\big) \ge 1-\epsilon_G, \quad \forall i \in \mathcal{N}_\mathcal{G} \tag{22}$$

$$\mathbb{P}\big(a\big(P_{G_i}(\mathbf{0}) + \boldsymbol{L}_{P(i,\cdot)}\boldsymbol{\xi}\big) + b\big(Q_{G_i}(\mathbf{0}) + \boldsymbol{L}_{Q(i,\cdot)}\boldsymbol{\xi}\big) \ge -S_{G_i}^{\max}\big) \ge 1-\epsilon_G, \quad \forall i \in \mathcal{N}_\mathcal{G} \tag{23}$$

$$\mathbb{P}\big(V_i(\mathbf{0}) + \boldsymbol{L}_{V(i,\cdot)}\boldsymbol{\xi} \le V_i^{\max}\big) \ge 1-\epsilon_V, \quad \forall i \in \mathcal{N} \tag{24}$$

$$\mathbb{P}\Big(V_i(\mathbf{0}) + \boldsymbol{L}_{V(i,\cdot)}\boldsymbol{\xi} \ge V_i^{\min}\Big) \ge 1-\epsilon_V, \quad \forall i \in \mathcal{N} \tag{25}$$

$$\mathbb{P}\big(\omega(\mathbf{0}) + \boldsymbol{L}_{\omega(1,\cdot)}\boldsymbol{\xi} \le \omega^{\max}\big) \ge 1-\epsilon_\omega, \tag{26}$$

$$\mathbb{P}\Big(\omega(\mathbf{0}) + \boldsymbol{L}_{\omega(1,\cdot)}\boldsymbol{\xi} \ge \omega^{\min}\Big) \ge 1-\epsilon_\omega, \tag{27}$$

where $a = \cos(m\frac{\pi}{16}), b = \sin(m\frac{\pi}{16}), m = 1,\ldots,16$ and the notations with subscript $(i,\cdot)$ refer to the i-th row of the respective matrices. Then, based on the property of Gaussian distribution, (20)–(27) are equivalent to the deterministic constraints as

$$P_{G_i}(\mathbf{0}) + \kappa_G \mathrm{Dev}\big\{P_{G_i}(\boldsymbol{\xi})\big\} \le S_{G_i}^{\max}, \quad \forall i \in \mathcal{N}_\mathcal{G} \tag{28}$$

$$P_{G_i}(\mathbf{0}) - \kappa_G \mathrm{Dev}\big\{P_{G_i}(\boldsymbol{\xi})\big\} \ge 0, \quad \forall i \in \mathcal{N}_\mathcal{G} \tag{29}$$

$$aP_{G_i}(\mathbf{0}) + bQ_{G_i}(\mathbf{0}) + \kappa_G \mathrm{Dev}\big\{aP_{G_i}(\boldsymbol{\xi}) + bQ_{G_i}(\boldsymbol{\xi})\big\} \le S_{G_i}^{\max}, \quad \forall i \in \mathcal{N}_\mathcal{G} \tag{30}$$

$$aP_{G_i}(\mathbf{0}) + bQ_{G_i}(\mathbf{0}) - \kappa_G \mathrm{Dev}\big\{aP_{G_i}(\boldsymbol{\xi}) + bQ_{G_i}(\boldsymbol{\xi})\big\} \ge -S_{G_i}^{\max}, \quad \forall i \in \mathcal{N}_\mathcal{G} \tag{31}$$

$$V_i(\mathbf{0}) + \kappa_V \mathrm{Dev}\{V_i(\boldsymbol{\xi})\} \le V_i^{\max}, \quad \forall i \in \mathcal{N} \tag{32}$$

$$V_i(\mathbf{0}) - \kappa_V \mathrm{Dev}\{V_i(\boldsymbol{\xi})\} \ge V_i^{\min}, \quad \forall i \in \mathcal{N} \tag{33}$$

$$\omega(\mathbf{0}) + \kappa_\omega \mathrm{Dev}\{\omega(\boldsymbol{\xi})\} \le \omega^{\max}, \tag{34}$$

$$\omega(\mathbf{0}) - \kappa_\omega \mathrm{Dev}\{\omega(\boldsymbol{\xi})\} \ge \omega^{\min}, \tag{35}$$

where $\kappa_G = \Phi^{-1}(1-\epsilon_G)$ denotes the inverse cumulative distribution function (CDF) of Gaussian distribution evaluated at $(1-\epsilon_G)$; similar interpretations apply to κ_V, κ_ω. According to the property of Gaussian distribution, the standard deviations can be described as follows

$$\begin{aligned}
&\mathrm{Dev}\{V_i(\boldsymbol{\xi})\} = \sqrt{\boldsymbol{L}_{V(i,\cdot)}\Sigma\big(\boldsymbol{L}_{V(i,\cdot)}\big)^T}, \quad \forall i \in \mathcal{N}\\
&\mathrm{Dev}\{P_{G_i}(\boldsymbol{\xi})\} = \sqrt{\boldsymbol{L}_{P(i,\cdot)}\Sigma(\boldsymbol{L}_{P(i,\cdot)})^T}, \quad \forall i \in \mathcal{N}_\mathcal{G}\\
&\mathrm{Dev}\big\{aP_{G_i}(\boldsymbol{\xi}) + bQ_{G_i}(\boldsymbol{\xi})\big\}\\
&= \sqrt{\big(a\boldsymbol{L}_{P(i,\cdot)} + b\boldsymbol{L}_{Q(i,\cdot)}\big)\Sigma\big(a\boldsymbol{L}_{P(i,\cdot)} + b\boldsymbol{L}_{Q(i,\cdot)}\big)^T}, \quad \forall i \in \mathcal{N}_\mathcal{G}\\
&\mathrm{Dev}\{\omega(\boldsymbol{\xi})\} = \sqrt{\boldsymbol{L}_{\omega(1,\cdot)}\Sigma\big(\boldsymbol{L}_{\omega(1,\cdot)}\big)^T},
\end{aligned} \tag{36}$$

From (28)–(35), we observe that the effect of renewable uncertainties in the chance constraint is equivalent to reducing the upper bound or increasing the lower bound by an uncertainty margin in the deterministic constraint.

C. Reformulation of CC-OPF-PFR

Similar to the transform of chance constraints, the objective function (9a) can be re-expressed as

$$\begin{aligned}
&\mathbb{E}\left[\sum_{i\in\mathcal{N}_\mathcal{G}} c_{2i}(P_{G_i}(\boldsymbol{\xi}))^2 + c_{1i}P_{G_i}(\boldsymbol{\xi}) + c_{0i}\right]\\
&= \sum_{i\in\mathcal{N}_\mathcal{G}} c_{2i}\Big[\big(P_{G_i}(\mathbf{0})\big)^2 + \boldsymbol{L}_{P(i,\cdot)}\Sigma\big(\boldsymbol{L}_{P(i,\cdot)}\big)^T\Big] + c_{1i}P_{G_i}(\mathbf{0}) + c_{0i}.
\end{aligned} \tag{37}$$

Then, the CC-OPF-PFR problem (9) can be reformulated as follows

$$\begin{aligned}
\text{minimize}\ \ & (37),\\
\text{subject to}\ \ & (9\text{b}) - (9\text{f}) \text{ for } \boldsymbol{\xi} = \mathbf{0},\\
& (9\text{o}) - (9\text{v}),\ (28) - (36).
\end{aligned} \tag{38}$$

As shown above, the standard deviation terms Dev$\{\cdot\}$ in (36) are determined by $\{\boldsymbol{V}, \boldsymbol{\theta}, \boldsymbol{T}^*, \boldsymbol{\beta}^*\}$. Obviously, $\boldsymbol{T}^*$ and $\boldsymbol{\beta}^*$ contribute more to the change of standard deviation terms Dev$\{\cdot\}$ than $\boldsymbol{V}$ and $\boldsymbol{\theta}$ because the per-unit values of voltage magnitudes are close to one and the voltage angles are close to zero in low voltage systems. To satisfy the more stringent constraints (28)-(35), traditional CC-OPF mainly relies on tuning the operating point by directly adjusting the power injections. However, from the perspective of network flexibility, we can expect that the PFRs not only tune the operating point but also reduce the standard deviations of voltage magnitudes (i.e., lower voltage volatility), which will be seen in the case studies.

If the sensitivity matrices $\boldsymbol{L}_P, \boldsymbol{L}_Q, \boldsymbol{L}_V, \boldsymbol{L}_\omega$ keep constant in (38), (38) becomes a deterministic OPF problem with flexible network parameters $\{\boldsymbol{T}^*, \boldsymbol{\beta}^*\}$. It can be solved by a modified SDP relaxation method [21]. However, as stated above, the sensitivity matrices are implicit and nonlinear functions of decision variables $\{\boldsymbol{V}, \boldsymbol{\theta}, \boldsymbol{T}^*, \boldsymbol{\beta}^*\}$, which makes problem (38) difficult to solve. To tackle this issue, we treat these sensitivity matrices as fixed coefficients in problem (38) at a given operating point $(\boldsymbol{V}, \boldsymbol{\theta}, \omega)$. In this case, the sensitivity matrices describe the changes of $\boldsymbol{P}_G, \boldsymbol{Q}_G, \boldsymbol{V}, \omega$ under certain

set points $\{\boldsymbol{P}_G^*, \boldsymbol{Q}_G^*, \omega^*, \boldsymbol{V}^*, \boldsymbol{T}^*, \boldsymbol{\beta}^*\}$ when the renewable outputs deviate from the forecasted values. By doing so, both the objective function and constraints take fully explicit expressions. More specifically, the quadratic terms associated with the system behaviours under renewable uncertainties, such as $\boldsymbol{L}_{P(i,\cdot)}\Sigma(\boldsymbol{L}_{P(i,\cdot)})^T$, will also become fixed coefficients in (38). For the chance constraints, these constant terms equivalently reduce the upper bounds or increase the lower bounds. For the objective function, the constant term $\boldsymbol{L}_{P(i,\cdot)}\Sigma(\boldsymbol{L}_{P(i,\cdot)})^T$ can be temporarily excluded. However, the problem is still not fully addressed after the above manipulations. It should be pointed out that the explicit expressions of the objective function and chance constraints in (38) describe the case of the given operating point rather than the optimal solution to (38). In other words, the optimal solution to (38) may not exactly satisfy the chance constraints since there is a mismatch between the standard deviation terms in (38) and their actual values at the optimal solution. Therefore, an iterative algorithm is required to gradually eliminate such kind of mismatch.

D. Iterative Solution Algorithm

For the convenience of algorithm statement, let us denote the uncertainty margin of V_i at the k-th iteration by $\Omega_{V_i}^k = \Phi^{-1}(1-\epsilon_V)\sqrt{\boldsymbol{L}_{V(i,\cdot)}^k\Sigma(\boldsymbol{L}_{V(i,\cdot)}^k)^T}$. Similar interpretations apply to $\Omega_{P_i}^k$, $\Omega_{PQ_i}^k$, Ω_ω^k and we define the vectors $\boldsymbol{\Omega}_P^k, \boldsymbol{\Omega}_{PQ}^k, \boldsymbol{\Omega}_V^k \in \mathbb{R}^n$ stacking $\Omega_{P_i}^k, \Omega_{PQ_i}^k, \Omega_{V_i}^k$, respectively. We summarize the iterative algorithm as follows.

Step 1: Initialize the iteration count $k = 0$, the sensitivity matrices $\boldsymbol{L}^0 = (\boldsymbol{L}_P^0, \boldsymbol{L}_Q^0, \boldsymbol{L}_V^0, L_\omega^0)$ and uncertainty margins $\boldsymbol{\Omega}^0 = (\boldsymbol{\Omega}_P^0, \boldsymbol{\Omega}_{PQ}^0, \boldsymbol{\Omega}_V^0)$ as zero matrices and $\Omega_\omega^0 = 0$.

Step 2: Solve subproblem (38) with fixed $\boldsymbol{L}^k$ and $\boldsymbol{\Omega}^k$ (e.g., by using SDP relaxation which will be introduced in the next subsection) and obtain the solution $\boldsymbol{x}^{k+1} = (\boldsymbol{V}^{k+1}, \boldsymbol{\theta}^{k+1}, \omega^{k+1}, \boldsymbol{P}_G^{*k+1}, \boldsymbol{Q}_G^{*k+1}, \omega^{*k+1}, \boldsymbol{V}^{*k+1}, \boldsymbol{T}^{*k+1}, \boldsymbol{\beta}^{*k+1})$.

Step 3: Calculate the sensitivity matrices $\boldsymbol{L}^{k+1} = (\boldsymbol{L}_P^{k+1}, \boldsymbol{L}_Q^{k+1}, \boldsymbol{L}_V^{k+1}, \boldsymbol{L}_\omega^{k+1})$ and the uncertainty margins $\boldsymbol{\Omega}^{k+1} = (\boldsymbol{\Omega}_P^{k+1}, \boldsymbol{\Omega}_{PQ}^{k+1}, \boldsymbol{\Omega}_V^{k+1}, \Omega_\omega^{k+1})$ at $\boldsymbol{x}^{k+1}$. Evaluate the maximum difference of $\boldsymbol{\Omega}$ between current iteration and the last iteration: $\Delta\boldsymbol{\Omega} = ||\boldsymbol{\Omega}^{k+1} - \boldsymbol{\Omega}^k||_\infty$.

Step 4 (Check convergence): If $\Delta\boldsymbol{\Omega} \le \delta$, stop. Otherwise, set $k = k+1$ and go back to Step 2.

The iterative algorithm converges when the maximum deviation of uncertainty margins is smaller than δ, which has a pre-defined value, e.g., 10^{-5}. The physical meaning of the converged solution is as follows: this solution takes the minimal cost to satisfy all the constraints, including those chance constraints in the form of (28)–(35) where the sensitivity matrices are obtained by the linearization around this solution.

As stated above, the iterative solution algorithm allows us to address the original CC-OPF problem (9) by iteratively solving the subproblem (38) with fixed uncertainty margins $\boldsymbol{\Omega}$, which retains the basic structure of deterministic AC-OPF and provides good scalability to different OPF solvers. Regarding the intractability induced by flexible network parameters in each subproblem, a modified SDP relaxation method is used which has been shown to be effective in handling similar optimization problems [21], [22]. In this way, we extend the iterative method in [23] to CC-OPF problems considering flexible network parameters. The effectiveness of the proposed method will be shown in the case studies. The next subsection will detail the SDP relaxation method.

E. SDP Relaxation

By adopting the modified SDP relaxation in [21], each subproblem (38) can be relaxed into a SDP form, which is detailed as follows. We introduce $\boldsymbol{W} = \vec{\boldsymbol{V}}_p\vec{\boldsymbol{V}}_p^H \in \mathbb{C}^{2l\times 2l}$ as an auxiliary matrix, where $\vec{\boldsymbol{V}}_p \in \mathbb{C}^{2l}$ is denoted as the column voltage vector by stacking $\vec{V}_{i_j} = V_{i_j}\angle\theta_{i_j}$ and $\vec{V}_{j_i} = V_{j_i}\angle\theta_{j_i}, \forall i \in \mathcal{N}, j \in \mathcal{N}_i$. The diagonal entry of $\boldsymbol{W}$ is defined as $W_{i_ji_j} = V_{i_j}^2, \forall i \in \mathcal{N}, j \in \mathcal{N}_i$ and the off-diagonal entry is defined as $W_{i_jk_l} = \vec{V}_{i_j}\vec{V}_{k_l}^H, \forall i,k \in \mathcal{N}, j \in \mathcal{N}_i, l \in \mathcal{N}_j$. Denote $W_{i_ji_j} = \Gamma_{i_j}W_i$ where $U_i = V_i^2$, $\Gamma_{i_j} = T_{i_j}^{*2}, \forall i \in \mathcal{N}, j \in \mathcal{N}_i$. Based on the above notations, problem (38) can be reformulated into an equivalent form in terms of $\boldsymbol{W}$ and $U_i, \forall i \in \mathcal{N}$, which is given as follows

$$\text{minimize} \quad \sum_{i\in\mathcal{N}_\mathcal{G}}\Big(c_{2i}\big(P_{G_i}(\mathbf{0})\big)^2 + c_{1i}P_{G_i}(\mathbf{0}) + c_{0i}\Big), \tag{39a}$$

$$\text{subject to} \quad \text{for } \boldsymbol{\xi} = \mathbf{0},$$

$$P_{G_i}(\boldsymbol{\xi}) + P_{W_i}(\boldsymbol{\xi}) - P_{L_i} + \mathrm{j}\big(Q_{G_i}(\boldsymbol{\xi}) + Q_{W_i}(\boldsymbol{\xi}) - Q_{L_i}\big) = \sum_{j\in\mathcal{N}_i}\big(W_{i_ji_j} - W_{i_ji_i}\big)y_{ij}^H, \forall i \in \mathcal{N} \tag{39b}$$

$$P_{G_i}(\boldsymbol{\xi}) = P_{G_i}^* + K_{p_i}^{-1}\big(\omega^* - \omega(\boldsymbol{\xi})\big), \forall i \in \mathcal{N}_\mathcal{G} \tag{39c}$$

$$Q_{G_i}(\boldsymbol{\xi}) = Q_{G_i}^* + K_{q_i}^{-1}(V_i^* - \frac{1}{2}(U_i+1)), \forall i \in \mathcal{N}_\mathcal{G} \tag{39d}$$

$$(9o) - (9r),\ (9v) \tag{39e}$$

$$T_{i_j}^{\min} = T_{i_j}^{\max} = T_{j_i}^{\min} = T_{j_i}^{\max} = 1,$$
$$\beta_{i_j}^{\min} = \beta_{i_j}^{\max} = \beta_{j_i}^{\min} = \beta_{j_i}^{\max} = 0^{\mathrm{o}}, \forall (i,j) \in \mathcal{E}^{\mathrm{norm}} \tag{39f}$$

$$U_i \le \big(V_i^{\max} - \Omega_{V_i}\big)^2, \forall i \in \mathcal{N} \tag{39g}$$

$$U_i \ge \Big(V_i^{\min} + \Omega_{V_i}\Big)^2, \forall i \in \mathcal{N} \tag{39h}$$

$$\Big(T_{i_j}^{\min}\Big)^2 U_i \le W_{i_ji_j} \le \Big(T_{i_j}^{\max}\Big)^2 U_i,$$
$$\Big(T_{j_i}^{\min}\Big)^2 U_j \le W_{j_ii_i} \le \Big(T_{j_i}^{\max}\Big)^2 U_j, \forall (i,j) \in \mathcal{E} \tag{39i}$$

$$\mathrm{Re}\big\{W_{i_ji_k}\big\}\tan\theta_{ji_k}^{\min} \le \mathrm{Im}\big\{W_{i_ji_k}\big\} \le \mathrm{Re}\big\{W_{i_ji_k}\big\}\tan\theta_{ji_k}^{\max}, \quad \forall i \in \mathcal{N}, j \ne k \in \mathcal{N}_i, \tag{39j}$$

$$\mathrm{Re}\big\{W_{i_ji_k}\big\} \ge T_{i_j}^{\min}T_{i_k}^{\max}U_i\cos\Big(\max\Big\{\Big|\theta_{ji_k}^{\min}\Big|, \Big|\theta_{ji_k}^{\max}\Big|\Big\}\Big), \quad \forall i \in \mathcal{N}, j \ne k \in \mathcal{N}_i, \tag{39k}$$

$$(28) - (31),\ (34) - (36), \tag{39l}$$

$$\boldsymbol{W} \succeq 0, \tag{39m}$$

$$\mathrm{rank}(\boldsymbol{W}) = 1. \tag{39n}$$

As mentioned in Section III-C, here we exclude the term $\boldsymbol{L}_{P(i,\cdot)}\Sigma(\boldsymbol{L}_{P(i,\cdot)})^T$ from the objective function (39a) since it

remains constant in each iteration. When the iterative algorithm converges, it will be added back to the objective function based on the value of $\boldsymbol{L}_P$ at the last iteration. Constraints (39b)–(39d) denote the power balance equations. Constraint (39f) ensures that T and β are always set to 1 and 0 for normal lines without PFRs, which is equivalent to (9u). Constraints (39g)–(39h) give the voltage constraints. Constraints (39i)–(39k) are designed to relax the non-convex constraints (6a)–(6b) and account for the equivalent tuning range of PFRs as shown in (9s)-(9t). We define $\theta_{ij i_k}^{\min} = \max\{\beta_{i_j}^{\min} - \beta_{i_k}^{\max}, -\pi/2\}$ and $\theta_{ij i_k}^{\max} = \min\{\beta_{i_j}^{\max} - \beta_{i_k}^{\min}, \pi/2\}$ as the lower and upper limits of the angular difference between $\vec{V}_{i_j}$ and $\vec{V}_{i_k}$, respectively. Constraint (39m) determines that $\boldsymbol{W}$ is positive semi-definite. Relaxing the rank constraint (39n) allows us to obtain an SDP problem which can be solved efficiently by off-the-shelf SDP solvers. It should be noted that SDP relaxation of the subproblem in each iteration is not an equivalence transformation. But studies in the literature [21], [37]–[39] have shown exact conditions and practical experience with the exactness of the solution obtained by SDP relaxation in the sense of equivalence to the solution to the original subproblem, i.e., constraint (39n) is satisfied. In this way, a globally optimal solution of (38) with fixed $\boldsymbol{\Omega}$ can be recovered from $\boldsymbol{W}^{\text{opt}}$ and $U_i^{\text{opt}}, \forall i \in \mathcal{N}$. In case of inexact relaxation, we can still enforce a rank-one solution by augmenting the objective function with a penalty term [39]. Here, the penalty function is chosen as a combination of a regularization term H_r proposed by [21], [40] and the total reactive power generation [39]. We replace the objective function (39a) by

$$\sum_{i\in\mathcal{N}_{\mathcal{G}}} \left(c_{2i}\big(P_{G_i}(\mathbf{0})\big)^2 + c_{1i}P_{G_i}(\mathbf{0}) + c_{0i}\right) + w_r H_r + w_q \sum_{i\in\mathcal{N}_{\mathcal{G}}} Q_{G_i}(\mathbf{0}) \tag{40}$$

where $H_r = \sum_{i\in\mathcal{N}} \sum_{j<k\in\mathcal{N}_i} (W_{ij i_j} + W_{ik i_k} - W_{ij i_k} - W_{ik i_j})$; w_r, w_q denote small positive numbers. Numerical examples [21], [39], [41] have shown the effectiveness of the adopted penalty terms for pursuing rank-one solutions with negligible effects on the optimality, which is also the situation in our case studies. By combining the SDP relaxation with the iterative solution algorithm, problem (9) is finally transformed into a small number of convex optimization problems, which can be efficiently solved by the existing SDP solvers.

F. Extension to Other Renewable PDFs

Note that the above method is based on the assumption that renewable PDFs are Gaussian distributions. But it is worth noting that the proposed analytical reformulation of chance constraints and objective function also applies if the renewable uncertainties follow some other types of symmetric PDFs. The only difference is that $\kappa_G, \kappa_V, \kappa_\omega$ will be determined by other distribution-dependent functions, such as (use κ_V as an example).

a) Student's t distributions: $\kappa_V = t_{\upsilon,\sigma_T}^{-1}(1-\epsilon_V)$ with zero mean, υ degrees of freedom and scale parameter $\sigma_T = (\upsilon-2)/\upsilon$.
b) Other arbitrary symmetric and unimodal distributions: $\kappa_V = (2/(9\epsilon))^{1/2}$, for $0 \le \epsilon \le 1/6$ [42].
c) Truncated Gaussian distributions: κ_V can be calculated based on the inverse CDF of the corresponding truncated distribution functions (see [43] for details).

Furthermore, our method is also likely to be extended to asymmetric PDFs, where we can approximate a certain asymmetric renewable PDF as a weighted sum of Gaussian distributions using a Gaussian mixture model (GMM) method [44]. Here, we use the voltage chance constraint as an example. Suppose the GMM of the renewable PDF is obtained below

$$\text{PDF}_{\boldsymbol{\xi}} = \sum_m w_m N(\mu_m, \Sigma_m) \tag{41}$$

where w_m is the weighted parameter; $N(\cdot)$ denotes the multivariate Gaussian distribution function with the corresponding mean vector μ_m and covariance matrix Σ_m. According to the linear relationship between $\Delta\boldsymbol{V}$ and $\Delta\boldsymbol{P}_W$ in (16) and [44, Proposition 1], the PDF of $\Delta V_i, \forall i \in \mathcal{N}$ takes the following form

$$\text{PDF}_{\Delta V_i} = \sum_m w_m N\Big(\boldsymbol{L}_{V(i,\cdot)}\mu_m, \boldsymbol{L}_{V(i,\cdot)}\Sigma_m \boldsymbol{L}_{V(i,\cdot)}^T\Big). \tag{42}$$

Then, we can obtain the uncertainty margin of $V_i, \forall i \in \mathcal{N}$, which is in terms of the inverse CDF of ΔV_i, e.g., using the method in [44]. In this way, the proposed method will be compatible to asymmetric renewable PDFs. A more systematic research along this direction will be considered in future works.

G. Extension to Grid-Connected MGs

Note that the above modeling and solution algorithm applies to islanded MGs with all DGs being fully inverter-based and droop-controlled. The proposed method can be extended to grid-connected MGs or islanded MGs with a large-sized synchronous generator. In that case, there is a slack bus that ensures a perfect steady-state system frequency (i.e., $\omega = 1$) and the proposed method needs to be modified accordingly. The related technical issues are shown as follows.

Considering a grid-connected MG with a slack bus, the system frequency is constant so that the P-ω droop control is no longer necessary. Without loss of generality, we assume bus 1 is the slack bus. If the forecast error of renewable power generation is not zero, the power mismatch $\sum_{i\in\mathcal{N}} \xi_i$ is shared among the dispatchable DGs according to the participation factors $\boldsymbol{\alpha} = [\alpha_i] \in \mathbb{R}^n$, where $\boldsymbol{\alpha}$ satisfies $\sum_{i\in\mathcal{N}} \alpha_i = 1$. The respective entries of $\boldsymbol{\alpha}$ are set to zero for the buses without dispatchable DGs.

Similar to (11), we can derive the linear relation between the change of power injections and the change of voltages as

$$\begin{bmatrix} \Delta\boldsymbol{P}_W^{\dagger} - \boldsymbol{\alpha}^{\dagger}\sum_{i\in\mathcal{N}}\xi_i \\ \Delta\boldsymbol{Q}_W^{\dagger} \\ 0 \end{bmatrix} = \boldsymbol{J}_{GC} \begin{bmatrix} \Delta\boldsymbol{\theta} \\ \Delta\boldsymbol{V}^{\dagger} \end{bmatrix}, \tag{43}$$

where the superscript $\dagger$ represents the vector whose first entry is eliminated, e.g., $\Delta\boldsymbol{P}_W^{\dagger} = [\Delta P_{W_2}, \Delta P_{W_3}, \ldots, \Delta P_{W_n}]$;

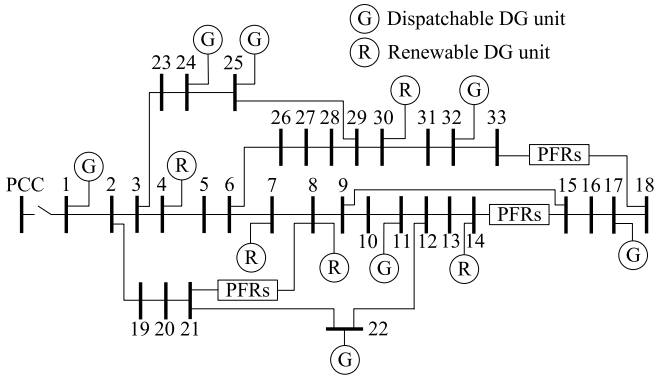

Fig. 2. The diagram of modified IEEE 33-bus MG.

$\boldsymbol{J}_{GC} \in \mathbb{R}^{(2n-1)\times(2n-1)}$ is the Jacobian matrix which can be expressed as

$$\boldsymbol{J}_{GC} = \begin{bmatrix} \boldsymbol{A}' & \boldsymbol{B}' \\ \boldsymbol{C}' & \boldsymbol{D}' + \boldsymbol{S}'_Q \\ \boldsymbol{e}_1 & \boldsymbol{0} \end{bmatrix}, \tag{44}$$

where $\boldsymbol{A}', \boldsymbol{C}' \in \mathbb{R}^{(n-1)\times n}$ is obtained by deleting the first row of the $\boldsymbol{A}$, $\boldsymbol{C}$ defined in (11); $\boldsymbol{B}', \boldsymbol{D}', \boldsymbol{S}'_Q \in \mathbb{R}^{(n-1)\times(n-1)}$ is obtained by deleting the first row and first column of the $\boldsymbol{B}$, $\boldsymbol{D}$, $\boldsymbol{S}_Q$ defined in (11). From the above equations we derive the expressions for the changes of voltages with respect to renewable power fluctuations

$$\begin{bmatrix} \Delta\boldsymbol{\theta} \\ \Delta\boldsymbol{V}^{\dagger} \end{bmatrix} = \boldsymbol{J}_{GC}^{-1} \begin{bmatrix} \Psi_a \\ \Psi_b \\ \boldsymbol{0} \end{bmatrix} \Delta\boldsymbol{P}_W, \tag{45}$$

where $\Psi_a = \text{diag}\{-\boldsymbol{\alpha}^{\dagger}\}\boldsymbol{1}_{\{n-1,n-1\}} + \boldsymbol{I}_{n-1}$ and $\Psi_b = \boldsymbol{\lambda}\boldsymbol{I}_{n-1}$; $\boldsymbol{1}_{\{n-1,n-1\}} \in \mathbb{R}^{(n-1)\times(n-1)}$ denotes a matrix with all elements being one; $\boldsymbol{I}_{n-1} \in \mathbb{R}^{(n-1)\times(n-1)}$ denotes the identity matrix. Comparing (15) with (45), the sensitivity matrices $\boldsymbol{L}_V$ with respect to grid-connected MGs can be obtained in a similar way. Then, the analytical reformulation, SDP relaxation, and iterative algorithm can still be carried out.

IV. Case Study

We use the modified IEEE 33-bus system shown in Fig. 2 to test the performance of the proposed CC-OPF-PFR model and the solution method. The line parameters and the loads follow the settings in Matpower [45]. PFRs are installed at lines (8,21), (14,15) and (18,33). To highlight the control effect, we set the parameters of lines with PFRs to be consistent with that of line (12,22). There are seven dispatchable DGs placed at buses 1, 11, 17, 22, 24, 25, 32 with $S_{G_i}^{\max} = 1.5$ MVA. Five renewable DGs are installed at buses 4, 7, 8, 14 and 30. Each renewable DG operates at the pre-defined power factor $\tan\phi_i = 0.95$. Their forecasted active power outputs are listed in Table I and the covariance matrix is given as follows

$$\Sigma = \begin{bmatrix} 0.0225 & 0.0024 & 0.0018 & 0.0015 & 0.0024 \\ 0.0024 & 0.0036 & 0.0009 & 0.0012 & 0.0018 \\ 0.0018 & 0.0009 & 0.0200 & 0.0015 & 0.0015 \\ 0.0015 & 0.0012 & 0.0015 & 0.0450 & 0.0021 \\ 0.0024 & 0.0018 & 0.0015 & 0.0021 & 0.0100 \end{bmatrix}.$$

TABLE I
Forecasted Renewable-Based DG Outputs (MW)

Bus	4	7	8	14	30
P_W	0.6	0.2	0.5	1.0	0.4

The total active power load of the system is 3.72 MW and the renewable penetration level is around 72.5%. Voltage limits for all the buses are set to $V_i^{\min} = 0.95$ and $V_i^{\max} = 1.05$. The PFR parameter specifications follow [27], particularly $T_{ij}^{\min} = T_{ji}^{\min} = 0.8$, $T_{ij}^{\max} = T_{ji}^{\max} = 2.5$, $\beta_{ij}^{\max} = \beta_{ji}^{\max} = -\beta_{ij}^{\min} = -\beta_{ji}^{\min} = 10^{\circ}$. The optimization computation is conducted on a 64-bit computer with 3.2 GHz CPU and 16 GB RAM. The optimization problem is solved by Mosek [46] via CVX [47] in MATLAB.

For comparison, we obtain the optimal solutions from the following four versions of OPF: (a) Normal OPF without PFRs and renewable uncertainties; (b) OPF-PFR (i.e., OPF with PFRs and without renewable uncertainties); (c) CC-OPF without PFRs; (d) CC-OPF-PFR.

For the base case, we set the violation probabilities as $\epsilon = \epsilon_G = \epsilon_V = \epsilon_\omega = 0.01$ and the tolerance value for convergence as $\delta = 10^{-5}$. Thus, the probability of satisfying the chance constraints is no less than 99%. The droop gains are set as $K_{Pi} = 3$ and $K_{Qi} = 30$ for dispatchable DGs.

To verify the proposed method, we also calculate the generation costs, empirical constraint violation probabilities and PDFs of voltage magnitudes by Monte Carlo Simulation (MCS). In the MCS, we calculate the AC power flow under 10^4 renewable output scenarios following the prescribed multivariate Gaussian distribution.

A. Merits of CC-OPF-PFR

We compare the generation costs, computational times, iteration numbers, and the maximum empirical violation probabilities Max.ϵ_{emp} of (a)–(d) and the results are listed in Table II. The obtained optimal tuning parameters for PFRs are shown in Table III. For methods (b) and (d), we first calculate the SDP relaxation (38) without penalty terms and the solutions (denoted by $f_l(x)$) are 2891.53 \$/hr and 2906.49 \$/hr, respectively. Then, the penalized objective function (40) is used to enforce a rank-one matrix $\boldsymbol{W}$ by choosing $w_r = 0.003$ and $w_q = 0.01$. Under the penalized objective function, the resulting generation costs (denoted by $f_u(x)$) of (b) and (d) are 2893.40 \$/hr and 2908.35 \$/hr, respectively. According to [41], the solutions $f_l(x)$ provide the lower bounds of the optimal values of (b) and (d), and the upper bounds are provided by $f_u(x)$. Thus, the global optimality guarantee can be assessed by $\frac{f_l(x)}{f_u(x)} \cdot 100\%$, which are 99.935% for (b) and 99.936% for (d). It means that the proposed SDP relaxation with penalty terms obtains a near-globally optimal solution whose distance to the global optimum is less than 0.1% of the obtained solution.

As shown in Table II, the iterative algorithm normally converges in 3 iterations and the computational time for two CC-OPF (c)–(d) problems are both within 10 seconds. This highlights the efficiency of the proposed iterative algorithm.

TABLE II
RESULTS OF THE FOUR OPF APPROACHES

Methods	(a)	(b)	(c)*	(d)*
Cost ($/hr)	2898.31	2893.40	2946.12	2908.35
CPU time (s)	1.04	3.33	4.04	9.94
Iterations	/	/	3	3
Max.$\epsilon^{\dagger}_{emp}$	42.46%	43.59%	0.79%	0.57%

*The costs of (c) and (d) include the term $\boldsymbol{L}_P\Sigma(\boldsymbol{L}_P)^T$ obtained at the last iteration.
†Max.ϵ_{emp} refers to the maximum empirical violation probability for all the constraints.

TABLE III
OPTIMAL VALUES OF PFR TUNING PARAMETERS

Location (i,j)	$T_{i_j}\angle\beta_{i_j}$
(8,21)	1.907 - 0.000i
(21,8)	1.910 - 0.000i
(14,15)	2.500 - 0.006i
(15,14)	2.498 - 0.009i
(18,33)	1.804 - 0.001i
(33,18)	1.811 - 0.002i

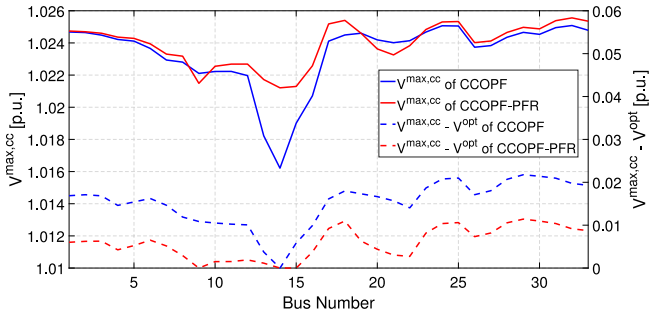

Fig. 3. $\boldsymbol{V}^{\max,cc} - \boldsymbol{V}^{opt}$ and equivalent voltage limits $\boldsymbol{V}^{\max,cc}$ in (38).

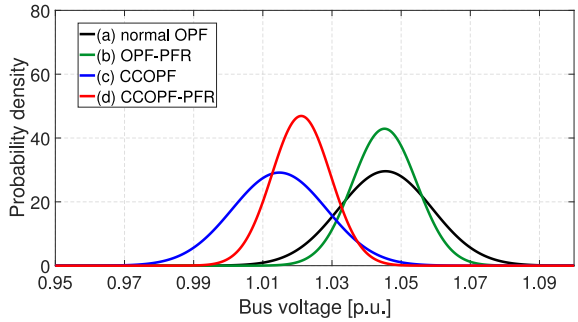

Fig. 4. Empirical voltage PDFs at bus 14 under (a)-(d) ($K_{Pi} = 3, K_{Qi} = 30$).

For the optimal solutions given by normal OPF and OPF-PFR, the maximum empirical violation probabilities are over 40%, which indicates the deterministic OPF is not sufficient to maintain an acceptable voltage profile under renewable uncertainties. By comparison, the maximum empirical violation probabilities under CC-OPF and CC-OPF-PFR are both consistent with the pre-specified violation probability (1%). This result verifies the effectiveness of chance constraints in securing the droop-controlled MGs against renewable uncertainties and the high accuracy of partial linearization on chance constraints. Similarly, we also evaluate the errors on generation costs induced by the partial linearization. According to the numerical results in the MCS, the mean values of generation costs under methods (c) and (d) are 2948.15 $/hr and 2911.04 $/hr, respectively. Compared the costs in Table II with the ones obtained by the MCS, we can see the errors of partial linearization on generation costs are only 0.07% and 0.09%, which are quite small and negligible. Moreover, the cost of CC-OPF-PFR is 1.28% lower the cost of CC-OPF and slightly higher than cost of normal OPF (0.35%). It shows that PFRs help the system in achieving better security without deteriorating much operational economy.

To detail the contribution of PFRs, we define $V_i^{\max,cc} = V_i^{\max} - \Omega_{V_i}$ as the equivalent voltage upper limit in voltage constraint (32) (i.e., $V_i(\mathbf{0}) \le V_i^{\max,cc}, \forall i \in \mathcal{N}$) when the iterative algorithm converges. Also, we denote $\boldsymbol{V}^{opt}$ as the voltage magnitudes at the optimal solution. Fig. 3 shows the values of $\boldsymbol{V}^{\max,cc}$ and $\boldsymbol{V}^{\max,cc} - \boldsymbol{V}^{opt}$ obtained by CC-OPF and CC-OPF-PFR, respectively. At most buses, the values of $\boldsymbol{V}^{\max,cc}$ under CC-OPF-PFR are higher than that under CC-OPF. It means that the voltage standard deviations of some buses are reduced by tuning $\boldsymbol{T}^*$ and $\boldsymbol{\beta}^*$ of the PFRs. In particular, we refer to bus 14 as the critical bus because (a) the standard deviation of V_{14} is dramatically reduce by PFRs; (b) its voltage magnitude hits the equivalent voltage limit (i.e., $V_{14}^{\max,cc} - V_{14}^{opt} = 0$) under both CC-OPF and CC-OPF-PFR. The hitting under CC-OPF (see the red dashed line) prevents the problem from seeking a further better solution along this direction; the hitting under CC-OPF-PFR (see the blue dashed line) means CC-OPF-PFR allows for pursuing a better solution due to the enlarged feasible region and this solution can be further improved by incorporating more network flexibility, i.e., more PFRs.

To further illustrate the effects of PFRs, the empirical voltage PDFs at bus 14 under (a)–(d) are shown in Fig. 4. By comparing (a) with (b) and (c) with (d), we observe that the empirical voltage PDFs have significantly narrower shapes if PFRs are included in the system. This is consistent with our previous analysis in Section III that tuning the PFR parameters $\boldsymbol{T}^*$ and $\boldsymbol{\beta}^*$ is effective in reducing the voltage standard deviations. Thus, the voltage volatility levels under OPF-PFR and CC-OPF-PFR are both lower than that without PFRs. Moreover, by comparing (a) with (c) and (b) with (d), we observe that the inclusion of chance constraints lead to left shifts of the mean values which are mainly achieved by power injection changes. On the other hand, the power injections do not make significant contribution to voltage volatility reduction as the PDF curves in (a) and (c) have almost the same shape. From the above discussion, we reveal that power injections and PFRs have different mechanisms in voltage regulation under uncertainties. Power injections mainly contribute to adjusting the mean values of voltage magnitudes, while PFRs mainly contribute to reducing the variances of voltage magnitudes. Therefore, the proposed CC-OPF-PFR outperforms the traditional CC-OPF by introducing a new dimension of control mechanism.

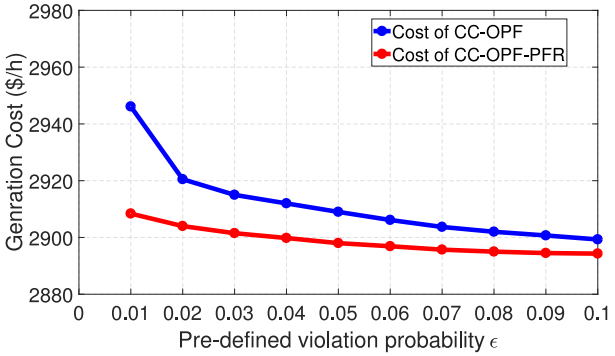

Fig. 5. Generation costs under different pre-defined violation probability ϵ.

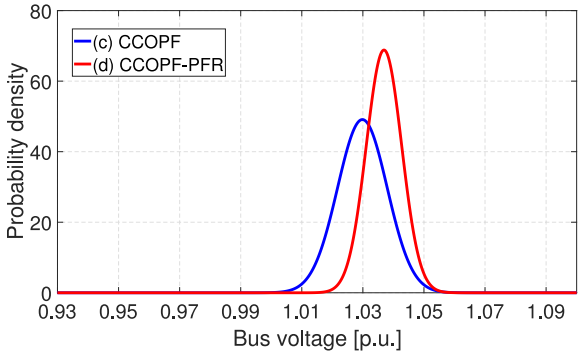

Fig. 6. Empirical voltage PDFs at bus 14 under (c) (d) ($K_{Pi} = 1, K_{Qi} = 10$).

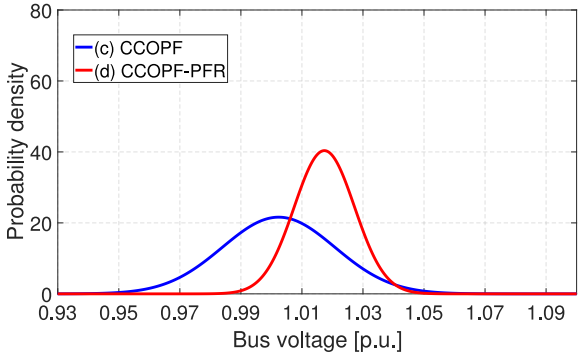

Fig. 7. Empirical voltage PDFs at bus 14 under (c) (d) ($K_{Pi} = 5, K_{Qi} = 50$).

B. Sensitivity Analysis w.r.t. Violation Probability ϵ

It is important to evaluate the impact of different pre-defined violation probabilities ϵ so that the system operators can make a trade-off between cost and security by choosing an appropriate value for ϵ. Here, we set the ϵ to be within [0.01, 0.1] in steps of 0.01. Then, based on the base case settings, we calculate the optimal generation costs of method (c)-(d) under different values of ϵ, as shown in Fig. 5.

As expected, the optimal generation costs of (c) and (d) both reduce as the value of ϵ increases, which means the system security is improved at the cost of higher generation cost. It is worth noting that the difference of generation costs under method (c) and (d) can be regarded as the benefits of PFRs. This difference also reduces as the value of ϵ increases. This is because when ϵ is small, more bus voltages hit the equivalent voltage limits (i.e., $V^{\text{opt}} = V^{\text{max,cc}}$). This kind of binding constraints limit the problem for pursuing a better solution. On the other hand, incorporating PFRs significantly reduces the uncertainty margins for voltage constraints, which allows for a better solution even if there still exist binding constraints. However, the benefits of PFRs become less significant as the increasing ϵ leads to less binding voltage constraints.

C. Performance Under Different Droop Gains

To further illustrate the merits of the CC-OPF-PFR model, we compare its performance with CC-OPF under another two types of droop gains in terms of generation costs, and voltage volatility. We set $K_{Pi} = 1, K_{Qi} = 10$ referring to low droop gains and $K_{Pi} = 5, K_{Qi} = 50$ referring to high droop gains.

1) Generation cost. For CC-OPF, the generation costs are 2918.18 \$/hr under low droop gains and 3049.37 \$/hr under high droop gains. For CC-OPF-PFR, the generation costs are 2903.40 \$/hr under low droop gains and 2925.74 \$/hr under high droop gains. We observe that higher droop gains lead to higher generation costs and this kind of cost increase is more notable for CC-OPF because it relies on tuning the power injections only. In addition, CC-OPF-PFR introduces 0.51% and 4.05% cost reduction compared to CC-OPF under low and high droop gains, respectively. This highlights the economic merits brought by PFRs under high droop gains, as the impact of renewable uncertainties on inducing more cost is also amplified by the high droop gains.

2) Voltage volatility. Similar to the previous subsection, Fig. 6 and Fig. 7 show the empirical voltage PDFs of bus 14 under low and high droop gains. We observe that the voltage volatilities are low for both CC-OPF and CC-OPF-PFR under low droop gains. However, under high droop gains, CC-OPF introduces a rather high voltage volatility level while CC-OPF-PFR still keeps a relatively small voltage volatility level.

We further discuss the results as follows.

(a) Under low droop gains, the voltage standard deviations $\text{Dev}\{\boldsymbol{V}(\boldsymbol{\xi})\}$ are naturally small. This property leads to small voltage margins $\boldsymbol{\Omega}_V$ and the chance constraints can be easily satisfied. Even with PFRs, their capabilities on $\text{Dev}\{\boldsymbol{V}(\boldsymbol{\xi})\}$ reduction by tuning $\boldsymbol{T}^*$ and $\boldsymbol{\beta}^*$ is limited to a small range. Therefore, the voltage volatility levels under CC-OPF and CC-OPF-PFR are similarly low as shown in Fig. 6.

(b) Under high droop gains, the voltage standard deviations $\text{Dev}\{\boldsymbol{V}(\boldsymbol{\xi})\}$ are relatively large and thus lead to more stringent voltage constraints (32)–(33). In this case, the value of PFRs is also amplified. Different from the CC-OPF which can only adjust the power injections to satisfy the constraints, PFRs can meet the voltage constraints by tuning $\boldsymbol{T}^*$ and $\boldsymbol{\beta}^*$ for smaller voltage standard deviations. Therefore, the voltage volatility under CC-OPF-PFR is much lower than that under CC-OPF as shown in Fig. 7. Furthermore, with the help of PFRs, the voltage volatility levels under high droop gains can even be close to the case under lower droop gains.

From the above discussion, we conclude that if high droop gains are adopted for islanded MGs, it could lead to serious volatile voltages under traditional CC-OPF. But the high droop

gains also amplify the capability of PFRs in reducing cost and voltage standard deviations. Therefore, the proposed CC-OPF-PFR has more significant merits under higher droop gains, which well matches the high droop gain nature of MGs.

V. Conclusion

In this paper, we propose a new CC-OPF-PFR problem in droop-controlled MGs under renewable uncertainties. In this formulation, the droop characteristics and PFRs are for the first time both considered in the CC-OPF model, where PFRs provide a new network-oriented mechanism different form the traditional node power control. Due to the complexity of AC power flow with PFRs, we extend an iterative solution method to be combined with an SDP relaxation method. By carrying out the power flow linearization around a given operating point, the CC-OPF-PFR problem can be addressed by iteratively solving a subproblem with flexible network parameters. Each subproblem is further relaxed into an SDP form so that the computationally tractability can be achieved. Numerical results show that the CC-OPF-PFR model significantly reduces the voltage volatility under high droop gains and achieves a highly secure solution with lower cost than the case without PFRs.

Many directions can be considered for future research, e.g., data-driven methods can be included for constructing the ambiguity set and distributionally robust optimization can be developed. Stability constraints need to be considered for a more robust and secure operating point. Moreover, corrective control of PFRs could be considered as a supplement to reduce the operational cost while maintaining the system security.

References

[1] M. Farrokhabadi *et al.*, "Microgrid stability definitions, analysis, and examples," *IEEE Trans. Power Syst.*, vol. 35, no. 1, pp. 13–29, Jan. 2020.

[2] J. M. Guerrero, J. C. Vasquez, J. Matas, L. G. De Vicuña, and M. Castilla, "Hierarchical control of droop-controlled AC and DC microgrids—A general approach toward standardization," *IEEE Trans. Ind. Electron.*, vol. 58, no. 1, pp. 158–172, Jan. 2011.

[3] E. Barklund, N. Pogaku, M. Prodanovic, C. Hernandez-Aramburo, and T. C. Green, "Energy management in autonomous microgrid using stability-constrained droop control of inverters," *IEEE Trans. Power Electron.*, vol. 23, no. 5, pp. 2346–2352, Sep. 2008.

[4] H. Han, X. Hou, J. Yang, J. Wu, M. Su, and J. M. Guerrero, "Review of power sharing control strategies for islanding operation of AC microgrids," *IEEE Trans. Smart Grid*, vol. 7, no. 1, pp. 200–215, Jan. 2016.

[5] Y. Song, D. J. Hill, T. Liu, and Y. Zheng, "A distributed framework for stability evaluation and enhancement of inverter-based microgrids," *IEEE Trans. Smart Grid*, vol. 8, no. 6, pp. 3020–3034, Nov. 2017.

[6] A. J. Wood, B. F. Wollenberg, and G. B. Sheblé, *Power Generation, Operation, and Control*. Hoboken, NJ, USA: Wiley, 2013.

[7] H. Zhang and P. Li, "Chance constrained programming for optimal power flow under uncertainty," *IEEE Trans. Power Syst.*, vol. 26, no. 4, pp. 2417–2424, Nov. 2011.

[8] Q. Wang, Y. Guan, and J. Wang, "A chance-constrained two-stage stochastic program for unit commitment with uncertain wind power output," *IEEE Trans. Power Syst.*, vol. 27, no. 1, pp. 206–215, Feb. 2012.

[9] L. M. Lopez-Ramos, V. Kekatos, A. G. Marques, and G. B. Giannakis, "Two-timescale stochastic dispatch of smart distribution grids," *IEEE Trans. Smart Grid*, vol. 9, no. 5, pp. 4282–4292, Sep. 2018.

[10] P. Li, B. Jin, D. Wang, and B. Zhang, "Distribution system voltage control under uncertainties using tractable chance constraints," *IEEE Trans. Power Syst.*, vol. 34, no. 6, pp. 5208–5216, Nov. 2019.

[11] F. U. Nazir, B. C. Pal, and R. A. Jabr, "A two-stage chance constrained volt/var control scheme for active distribution networks with nodal power uncertainties," *IEEE Trans. Power Syst.*, vol. 34, no. 1, pp. 314–325, Jan. 2019.

[12] M. Vrakopoulou, B. Li, and J. L. Mathieu, "Chance constrained reserve scheduling using uncertain controllable loads Part I: Formulation and scenario-based analysis," *IEEE Trans. Smart Grid*, vol. 10, no. 2, pp. 1608–1617, Mar. 2019.

[13] A. Hassan, R. Mieth, M. Chertkov, D. Deka, and Y. Dvorkin, "Optimal load ensemble control in chance-constrained optimal power flow," *IEEE Trans. Smart Grid*, vol. 10, no. 5, pp. 5186–5195, Sep. 2019.

[14] E. Dall'Anese, K. Baker, and T. Summers, "Chance-constrained AC optimal power flow for distribution systems with renewables," *IEEE Trans. Power Syst.*, vol. 32, no. 5, pp. 3427–3438, Sep. 2017.

[15] Y. Jiang, C. Wan, J. Wang, Y. Song, and Z. Y. Dong, "Stochastic receding horizon control of active distribution networks with distributed renewables," *IEEE Trans. Power Syst.*, vol. 34, no. 2, pp. 1325–1341, Mar. 2019.

[16] J. Li, F. Liu, Z. Li, C. Shao, and X. Liu, "Grid-side flexibility of power systems in integrating large-scale renewable generations: A critical review on concepts, formulations and solution approaches," *Renew. Sustain. Energy Rev.*, vol. 93, pp. 272–284, Oct. 2018.

[17] L. Roald, S. Misra, T. Krause, and G. Andersson, "Corrective control to handle forecast uncertainty: A chance constrained optimal power flow," *IEEE Trans. Power Syst.*, vol. 32, no. 2, pp. 1626–1637, Mar. 2017.

[18] A. Venzke and S. Chatzivasileiadis, "Convex relaxations of probabilistic AC optimal power flow for interconnected AC and HVDC grids," *IEEE Trans. Power Syst.*, vol. 34, no. 4, pp. 2706–2718, Jul. 2019.

[19] A. Venzke, L. Halilbašić, A. Barré, L. Roald, and S. Chatzivasileiadis, "Chance-constrained AC optimal power flow integrating HVDC lines and controllability," *Int. J. Elect. Power Energy Syst.*, vol. 116, Mar. 2020, Art no. 105522.

[20] P. G. Thakurta, R. Belmans, and D. Van Hertem, "Risk-based management of overloads caused by power injection uncertainties using power flow controlling devices," *IEEE Trans. Power Syst.*, vol. 30, no. 6, pp. 3082–3092, Nov. 2015.

[21] J. Lin, V. O. K. Li, K.-C. Leung, and A. Y. S. Lam, "Optimal power flow with power flow routers," *IEEE Trans. Power Syst.*, vol. 32, no. 1, pp. 531–543, Jan. 2017.

[22] T. Chen, A. Y. S. Lam, Y. Song, and D. J. Hill, "Reducing BESS capacity for accommodating renewables in subtransmission systems with power flow routers," in *Proc. Int. Conf. Smart Grids Energy Syst. (SGES)*, Perth, WA, Australia, 2020, pp. 584–589.

[23] L. Roald and G. Andersson, "Chance-constrained AC optimal power flow: Reformulations and efficient algorithms," *IEEE Trans. Power Syst.*, vol. 33, no. 3, pp. 2906–2918, May 2018.

[24] Z. Li, J. Wang, H. Sun, F. Qiu, and Q. Guo, "Robust estimation of reactive power for an active distribution system," *IEEE Trans. Power Syst.*, vol. 34, no. 5, pp. 3395–3407, Sep. 2019.

[25] L. Roald, F. Oldewurtel, T. Krause, and G. Andersson, "Analytical reformulation of security constrained optimal power flow with probabilistic constraints," in *Proc. IEEE Grenoble Conf.*, Grenoble, France, 2013, pp. 1–6.

[26] D. Bienstock, M. Chertkov, and S. Harnett, "Chance-constrained optimal power flow: Risk-aware network control under uncertainty," *SIAM Rev.*, vol. 56, no. 3, pp. 461–495, 2014.

[27] T. Chen, A. Y. S. Lam, Y. Song, and D. J. Hill, "Robust transient stability constrained optimal power flow with power flow routers considering renewable uncertainties," 2020, *arXiv:2006.00506*.

[28] A. Q. Huang, M. L. Crow, G. T. Heydt, J. P. Zheng, and S. J. Dale, "The future renewable electric energy delivery and management (FREEDM) system: The energy Internet," *Proc. IEEE*, vol. 99, no. 1, pp. 133–148, Jan. 2011.

[29] M. M. A. Abdelaziz, H. E. Farag, E. F. El-Saadany, and Y. A.-R. I. Mohamed, "A novel and generalized three-phase power flow algorithm for islanded microgrids using a Newton trust region method," *IEEE Trans. Power Syst.*, vol. 28, no. 1, pp. 190–201, Feb. 2013.

[30] F. Mumtaz, M. H. Syed, M. A. Hosani, and H. H. Zeineldin, "A novel approach to solve power flow for islanded microgrids using modified Newton Raphson with droop control of DG," *IEEE Trans. Sustain. Energy*, vol. 7, no. 2, pp. 493–503, Apr. 2016.

[31] M. H. Moradi, V. B. Foroutan, and M. Abedini, "Power flow analysis in islanded micro-grids via modeling different operational modes of DGs: A review and a new approach," *Renew. Sustain. Energy Rev.*, vol. 69, pp. 248–262, Mar. 2017.

[32] M. M. A. Abdelaziz, H. E. Farag, and E. F. El-Saadany, "Optimum droop parameter settings of islanded microgrids with renewable energy resources," *IEEE Trans. Sustain. Energy*, vol. 5, no. 2, pp. 434–445, Apr. 2014.
[33] M. M. A. Abdelaziz, H. E. Farag, and E. F. El-Saadany, "Optimum reconfiguration of droop-controlled islanded microgrids," *IEEE Trans. Power Syst.*, vol. 31, no. 3, pp. 2144–2153, May 2016.
[34] P. P. Vergara, J. C. López, M. J. Rider, and L. C. Da Silva, "Optimal operation of unbalanced three-phase islanded droop-based microgrids," *IEEE Trans. Smart Grid*, vol. 10, no. 1, pp. 928–940, Jan. 2019.
[35] Y. Zhang, S. Shen, and J. L. Mathieu, "Distributionally robust chance-constrained optimal power flow with uncertain renewables and uncertain reserves provided by loads," *IEEE Trans. Power Syst.*, vol. 32, no. 2, pp. 1378–1388, Mar. 2017.
[36] C. Duan, W. Fang, L. Jiang, L. Yao, and J. Liu, "Distributionally robust chance-constrained approximate AC-OPF with Wasserstein metric," *IEEE Trans. Power Syst.*, vol. 33, no. 5, pp. 4924–4936, Sep. 2018.
[37] S. H. Low, "Convex relaxation of optimal power flow—Part I: Formulations and equivalence," *IEEE Trans. Control Netw. Syst.*, vol. 1, no. 1, pp. 15–27, Mar. 2014.
[38] S. H. Low, "Convex relaxation of optimal power flow—Part II: Exactness," *IEEE Trans. Control Netw. Syst.*, vol. 1, no. 2, pp. 177–189, Jun. 2014.
[39] R. Madani, S. Sojoudi, and J. Lavaei, "Convex relaxation for optimal power flow problem: Mesh networks," *IEEE Trans. Power Syst.*, vol. 30, no. 1, pp. 199–211, Jan. 2015.
[40] B. Recht, M. Fazel, and P. A. Parrilo, "Guaranteed minimum-rank solutions of linear matrix equations via nuclear norm minimization," *SIAM Rev.*, vol. 52, no. 3, pp. 471–501, 2010.
[41] R. Madani, M. Ashraphijuo, and J. Lavaei, "Promises of conic relaxation for contingency-constrained optimal power flow problem," *IEEE Trans. Power Syst.*, vol. 31, no. 2, pp. 1297–1307, Mar. 2016.
[42] L. Roald, F. Oldewurtel, B. Van Parys, and G. Andersson, "Security constrained optimal power flow with distributionally robust chance constraints," 2015, *arXiv:1508.06061*.
[43] J. Burkardt, *The Truncated Normal Distribution*, Dept. Sci. Comput., Florida State Univ., Tallahassee, FL, USA, 2014, pp. 1–35.
[44] Z. Wang, C. Shen, F. Liu, X. Wu, C.-C. Liu, and F. Gao, "Chance-constrained economic dispatch with non-Gaussian correlated wind power uncertainty," *IEEE Trans. Power Syst.*, vol. 32, no. 6, pp. 4880–4893, Nov. 2017.
[45] R. D. Zimmerman, C. E. Murillo-Sánchez, and R. J. Thomas, "MATPOWER: Steady-state operations, planning, and analysis tools for power systems research and education," *IEEE Trans. Power Syst.*, vol. 26, no. 1, pp. 12–19, Feb. 2011.
[46] (MOSEK ApS, Copenhagen, Denmark). *The MOSEK Optimization Toolbox for MATLAB Manual. Version 9.0*, (2019). [Online]. Available: http://docs.mosek.com/9.0/toolbox/index.html
[47] M. Grant and S. Boyd. "CVX: MATLAB Software for Disciplined Convex Programming, Version 2.1." Mar. 2014. [Online]. Available: http://cvxr.com/cvx

Tianlun Chen (Member, IEEE) received the B.E. degree from Zhejiang University, Hangzhou, China, in 2016. He is currently pursuing the Ph.D. degree with the Department of Electrical and Electronic Engineering, The University of Hong Kong. His research interests include stability and optimization of energy network systems.

Yue Song (Member, IEEE) received the B.S. and M.S. degrees in electrical engineering from Shanghai Jiao Tong University in 2011 and 2014, respectively, and the Ph.D. degree in electrical engineering from The University of Hong Kong (HKU), in 2017, where he was a Postdoctoral Fellow from September 2017 to April 2020. He is currently a Research Assistant Professor with the Department of Electrical and Electronic Engineering, HKU. His research interests include stability, optimization, and control of energy network systems.

David J. Hill (Life Fellow, IEEE) received the B.E. degree in electrical engineering and the B.Sc. degree in mathematics from the University of Queensland, Australia, in 1972 and 1974, respectively, and the Ph.D. degree in electrical engineering from the University of Newcastle, Australia, in 1976.

He is a Professor of Energy Systems with The University of New South Wales, Sydney. He was the Chair of Electrical Engineering and the Director of the Centre for Electrical Energy Systems, The University of Hong Kong and is currently a Professor Emeritus. He was also a part-time Professor with The University of Sydney and is currently a Professor Emeritus. His general research interests are in control systems, complex networks, power systems and stability analysis. Currently, his work is mainly on control and planning of future energy networks and basic stability and control questions for dynamic networks. He is a Fellow of the Society for Industrial and Applied Mathematics, the International Federation of Automatic Control, the Australian Academy of Science and the Australian Academy of Technological Sciences and Engineering. He is also a Foreign Member of the Royal Swedish Academy of Engineering Sciences.

Albert Y. S. Lam (Senior Member, IEEE) received the B.Eng. degree (First Class Hons.) in information engineering and the Ph.D. degree in electrical and electronic engineering from the University of Hong Kong (HKU), Hong Kong, in 2005 and 2010, respectively. He was a Postdoctoral Scholar with the Department of Electrical Engineering and Computer Sciences, University of California, Berkeley, CA, USA, from 2010 to 2012. He is currently the Chief Scientist and the Chief Technology Officer with Fano Labs, and an Adjunct Assistant Professor with the Department of Electrical and Electronic Engineering and the Department of Geography, HKU. He is a Croucher Research Fellow. His research interests include optimization theory and algorithms, artificial intelligence, smart grid, and smart city. He is an Associate Editor of IEEE TRANSACTIONS ON INTELLIGENT TRANSPORTATION SYSTEMS and IEEE TRANSACTIONS ON EVOLUTIONARY COMPUTATION.